TMR and Al-O Based Magnetic Tunneling Junctions

5

Xiu-Feng Han

Contents

X.-F. Han (✉)
Chinese Academy of Sciences, State Key Laboratory of Magnetism, Institute of Physics, Beijing, China
e-mail: xfhan@aphy.iphy.ac.cn

Y. Xu et al. (eds.), *Handbook of Spintronics*,
DOI 10.1007/978-94-007-6892-5_10

Abstract

AlO_x is the most typical barrier material in the early research of high tunneling magneto-resistance (TMR) in magnetic tunnel junctions (MTJs) at room temperature (RT). AlO_x is easily formed by oxidizing a pre-deposited Al layer. The MTJ with FM/I/FM sandwich core structure and the spin-dependent tunneling transport properties drew a wide range of interest resulting the so far largest magnetoresistance (MR) ratio of 81% at RT and 107% at 4.2 K in AlO_x based tunnel junction. The different types of Al-O barrier based MTJs are Sandwich-Structured MTJ, Spin-Valve Type Pinned MTJ, Double Barrier Magnetic Tunnel Junction (DBMTJ), Half-Metal MTJ, Perpendicular Anisotropic MTJ, Dilute Magnetic Semiconductors Composite MTJ, Superconductors Composite MTJ, Granular Film Composite MTJ and Nano-Ring-Shaped MTJ. A lot of research has been done in this field regarding its practical application in devices and technology. Furthermore, the discovery of Spin-transfer torque (STT) effect is a remarkable achievement in the development process and rapid emergence of spintronics. This effect provides not only a new data writing strategy, but is also consistent with the development trend of high density devices. To reduce the critical switching current is the pursuing target both in lab and industry. The important applications of Al–O based MTJs including Magnetic Read Heads, Magnetic Sensors, Magnetic Random Access Memory (MRAM), Spin Transistors and Field Effect Transistors, Magnetic Logic Devices and Memristors will be discussed in details in this chapter to provide an advanced technological understanding to the readers.

Introduction with Historical Background of Al–O Based MTJs

The core cell of a simplest magnetic tunnel junction (MTJ) is composed of an insulating layer sandwiched between two magnetic layers. The tunnel resistances of MTJ are different with respect to the relative orientation of magnetic moments of the two ferromagnetic layers known as the tunneling magnetoresistance (TMR) effect. In 1975, TMR effect was first observed by French scholar named Julliére in Fe/Ge/Co multilayer [1], who proposed phenomenological model based on the "ferromagnetic electrode (FM)/insulator (I)/ferromagnetic electrode (FM)" core structure MTJ. The key points of Julliére's model are: the TMR ratio is determined by the spin polarization of two ferromagnetic electrodes and is irrelevant with the insulator layer; and the spin of electrons are conserved during the tunnel process. When the magnetic moments of two ferromagnetic electrodes are aligned parallel, the electrons with majority-spin in one ferromagnetic electrode will tunnel into the

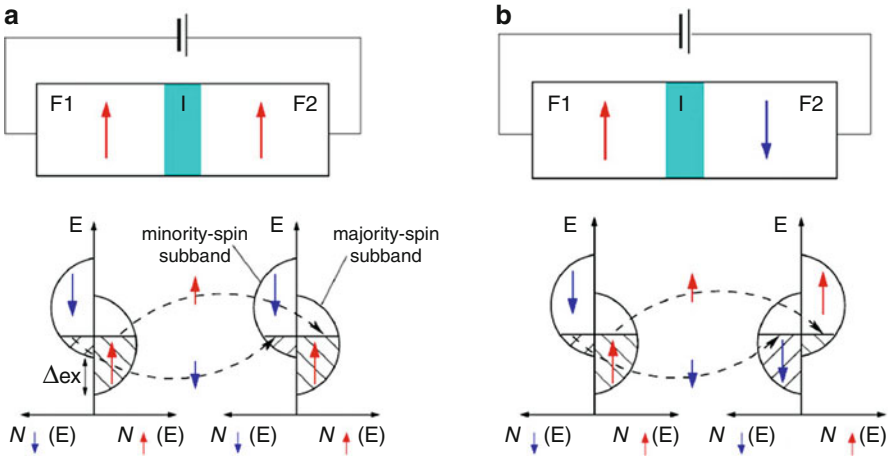

Fig. 1 Schematic of electrons tunneling in FM/I/FM MTJs: (**a**) parallel and (**b**) antiparallel magnetization orientations with the corresponding spin resolved density of the *d* states in ferromagnetic metals that have exchanged spin splitting Δ_{ex}. *Arrows* in the two ferromagnetic regions are determined by the majority-spin sub-band. *Dashed lines* depict spin conserved tunneling (Reprinted with permission from [5]. Copyright (2004) by the American Physical Society)

unoccupied majority-spin sub-band in the other ferromagnetic electrode. Similarly the electrons with minority-spin will tunnel into the unoccupied state of minority-spin sub-band, which yield a lower tunnel magnetic junction resistance, as shown in Fig. 1a. When the magnetic moments of two ferromagnetic electrodes are aligned antiparallel, the electrons of majority-spin sub-band in one ferromagnetic electrode can only tunnel into the unoccupied state of minority-spin sub-band in other electrode and the electrons in minority-spin sub-band will only tunnel into the unoccupied state of majority-spin sub-band, which limits the total number of electrons participating in transport and results in a higher tunnel magnetic junction resistance, as shown in Fig. 1b. Thus, within the Julliére's model, the TMR ratio is defined as: $\mathrm{TMR} = (G_P - G_{AP})/G_{AP} = 2P_1P_2/(1-P_1P_2)$, where G_P and G_{AP} are conductances under parallel and antiparallel states, respectively, and P_i is the spin polarization of ferromagnetic electrode i, which is defined as, $P_i = (D_{i\uparrow} - D_{i\downarrow})/(D_{i\uparrow} + D_{i\downarrow})$ where, $D_{i\uparrow}$ and $D_{i\downarrow}$ are density of states at Fermi level for the majority- and minority- spins, respectively. Julliére's model predicts that using high spin polarization metal and metallic alloy materials could yield a large TMR ratio, which agrees well with the earlier experimental results. However, limited by the experimental conditions, during 1970s and 1980s, high quality MTJ multilayers could not be obtained. No significant progress had been achieved and no room temperature TMR effect was reported, so very less attention was paid on MTJ during this 20 years.

The MTJ with FM/I/FM sandwich core structure and the spin-dependent tunneling transport properties drew a wide range of interest and in-depth study in both experimental and theoretical research fields after the report of large TMR ratio of

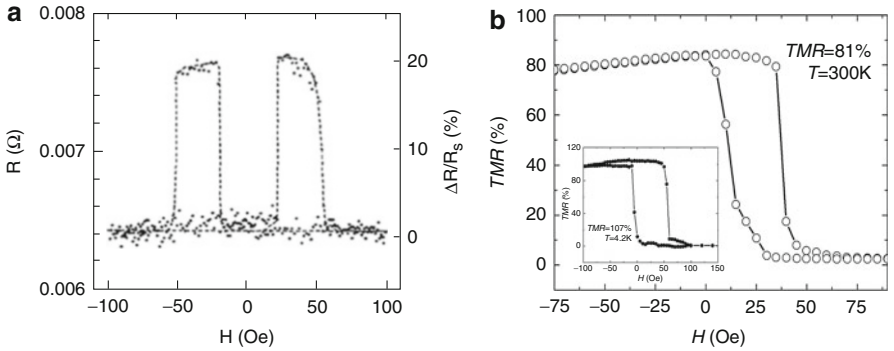

Fig. 2 (**a**) The large TMR at room temperature observed by Miyazaki et al. [2, 3] in MTJs using amorphous aluminum oxide as barrier (Reprinted from [2]. Copyright (1995) with permission from Elsevier). (**b**) TMR of 81 % at room temperature observed by Wei et al. [4] in ring-shaped MTJ with core structure of CoFeB/Al–O/CoFeB (Reprinted with permission from [4]. Copyright (2007), AIP Publishing LLC)

20 % at room temperature achieved independently in magnetic tunnel junction by Miyazaki et al. [2] and Moodera et al. [3], where the amorphous aluminum oxide (AlO_x) was used as the barrier. So far, the largest magnetoresistance (MR) ratio of AlO_x based tunnel junction is 81 % and is discovered in ring-shaped MTJ with core structure of CoFeB/Al–O/CoFeB [4], as indicated in Fig. 2b.

In the aspect of fabricating magnetic tunnel junction, much effort has been made on optimizing the ferromagnetic electrode materials in order to gain a larger TMR. Various magnetic materials were adopted as electrodes to explore the physical properties and enlarge the potential applications of AlO_x based tunnel junction. Magnetic semiconductors like Ga(Mn,As) have been used as magnetic electrode in hybrid MTJs [6, 7]. Superconductors as part of hybrid magnetic electrode are adopted in superconductor-ferromagnet hybrid tunnel junction [8]. And magnetic films with perpendicular magnetic anisotropy are also adopted as magnetic electrode to fabricate perpendicular magnetic tunnel junction (p-MTJ).

Referring to the structure of MTJ, besides the single barrier MTJ (FM/I/FM), double barrier tunnel junction (FM/I/FM/I/FM) also exhibits enhanced physical properties with wide applications. In double barrier magnetic tunnel junction (DBMTJ), oscillatory TMR and resonant tunneling is predicted for quantum well states [9]. Experimentally, double barrier MTJs of pseudo-spin valve and spin valve structures were first fabricated by Montaigne et al. [10] and Saito et al. [11], respectively. Both of them examined bias dependence of TMR in the above mentioned MTJs. New spin dependent transport phenomenon, know as Coulomb blockade magnetoresistance (CBMR), was observed by inserting a discontinuous or granular ferromagnetic layer in between double barriers of MTJ [12]. Besides the double barrier tunnel junction, quantum well state and resonant tunneling could also be observed in FM/NM/I/FM single barrier tunnel junction. In such configurations, an appropriate non-magnetic metal layer is inserted between one ferromagnetic

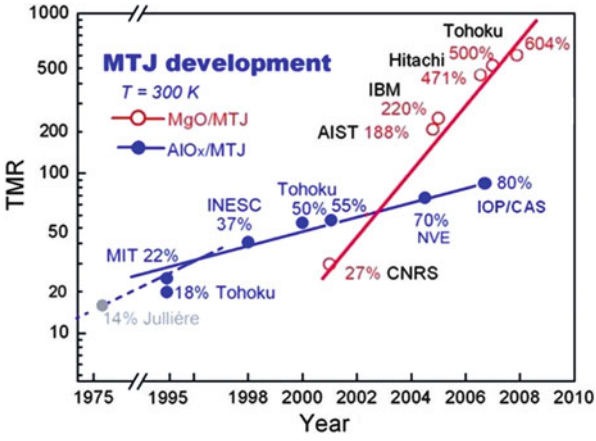

Fig. 3 The development road-map of single barrier MTJ with AlO_x, MgO, and other barrier materials

electrode and AlO_x barrier. After multiple reflections at the FM/NM interface, conduction electrons from the quantum well state of non-magnetic layer will tunnel as a result of resonance. The TMR ratio will oscillate as a function of the thickness of non-magnetic layer.

In 2004, Huai et al. observed the clear evidence of spin transfer torque in Al–O based MTJs for the first time [13]. This work further verifies the spin transfer torque effect predicted in nano- multilayered structures by early theorists [14, 15]. Spin transfer torque is a new kind of quantum effect which have been distinguished from the giant magnetoresistance (GMR) and TMR. The discovery of spin transfer torque in MTJ not only provides a new approach to switch magnetization in thin films by spin polarized current but also makes the design of high frequency MTJ-based devices such as spin nano-oscillator and spin microwave detector (Fig. 3).

Besides being used in various magnetic sensors, AlO_x based magnetic tunnel junction has played a landmark influence on the development of computer magnetic read head and magnetic high-density storage technology. AlO_x based MTJ is the first class of elements successfully being used in magnetic random access memory (MRAM) cell design and manufacture, for example the 1 M [16] and 16 M [17] field-driven MRAM. Various spintronic devices such as spin transistor and magnetic logic devices based on AlO_x barrier tunnel junctions are still being widely proposed [18].

Growth and Fabrication of Al–O Based MTJ

In the research of the TMR effect, the micro-fabrication or nanofabrication of multilayer-MTJs is crucial for the investigation of MTJs as well as the applications of MTJ devices. The process of fabrication of AlO_x based MTJ roughly consists of: deposition of magnetic multilayer films, fabrication of MTJs using contact shadow masks, fabrication of MTJs by photolithography combined with ion-beam etching,

fabrication of nano-MTJs using electron beam lithography (EBL) combined with ion-beam etching, fabrication of MTJs combined with focused ion beam (FIB), oxidation of aluminum, and the thermal treatment of MTJs. In MTJs' fabrication, all of the steps, either depositing multilayer films or the subsequent micro-fabrication, are related to the final device performance. The most crucial steps are the deposition and oxidation of aluminum and the thermal treatment of MTJs. In view of the chapter length, rather than giving the details of processing technology, major emphasis has been given on the oxidation of aluminum and the thermal treatment of MTJs.

In the early research of high TMR in MTJs at room temperature, AlO_x is the most typical barrier material. AlO_x is formed by oxidizing a pre-deposited Al layer. In previous experiments, the oxidation is usually carried out by natural oxidation [2, 3, 19–22] or plasma oxidation [4, 20, 23–27]. For natural oxidation, after the deposition of Al film, Al is oxidized in the chamber filled with oxygen at a certain pressure. The disadvantages of natural oxidation are: long time of oxidation, non-uniformity, low TMR ratio, difficulty of controlling resistance area product (RA), and inadequacy for large-scale industrialization. In comparison, plasma oxidation has the advantages of short time process, uniformity, and adjustable pressure of oxygen and power. So optimization of oxidizing condition is required for different equipments to obtain high TMR ratio in MTJs. The plasma oxidation can be used for large-scale industrialization. The highest TMR ratio achieved so far, by plasma oxidation of AlOx barrier in MTJs, is 81 % [4]. In addition to the two methods mentioned above, radical oxidation [28] and ultraviolet light assisted oxidation [29–31] has also been proposed previously. It is reported by Shimazawa et al. that the RA of MTJs can be decreased and the breakdown voltage can be increased by radical oxidation [28]. By using an ultraviolet light assisted oxidation process, it was observed that the bias voltage dependence [29] is improved and impurities in the barrier can be reduced [30].

Figure 4a [32] shows the impact of different oxidation time on TMR ratio in AlO_x-based MTJs. With the increase in Al thickness, the TMR ratio first increases and reaches a maximum value and then decreases again. This behavior of junction corresponds over-oxidation to under-oxidization of the aluminum. It was observed that both types of oxidizations can reduce the TMR ratio in MTJs. Therefore, proper thickness and oxidation time is very crucial for fabricating MTJs with high TMR ratio. Based on the average phase profile perpendicular to the barrier, as shown in Fig. 4b–d, it is suggested that a sharp interface can be achieved in optimally oxidized junctions [33].

Previous work has shown that the TMR in AlO_x-based MTJs can be increased by thermal annealing [20, 24, 25, 27, 34–40]. Parkin et al. suggested that the increased MR during annealing is related to homogenization of the tunnel barrier or, more likely, an improved interface with the ferromagnetic layer [20]. After reaching the maximum, the TMR ratio decreases when temperature is continuously increased, which is attributed to the oxidation of the ferromagnetic electrodes. The interdiffusion of Mn, from the antiferromagnetic IrMn layer used to pin the top electrode of the junction, is also responsible for the structural changes at the ferromagnetic layer/AlO_x interface [25, 34, 35, 38].

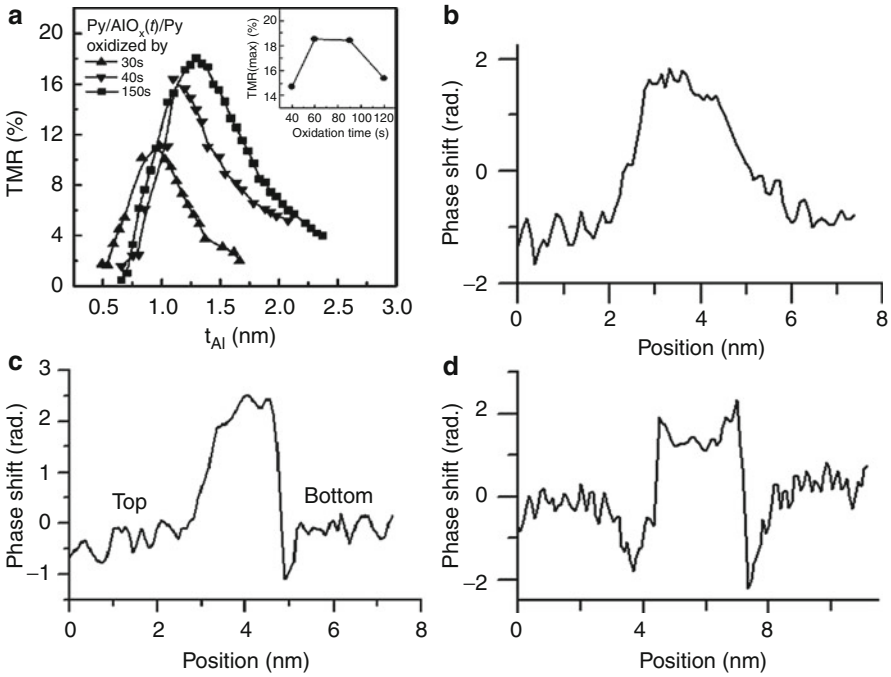

Fig. 4 (**a**) TMR ratio versus Al thickness in Py/AlO$_x$(t)/Py with wedge-shaped Al layers oxidized for 30, 40, and 150 s (Reprinted with permission from [32]. Copyright (2002) by the American Physical Society). The inset plots the maximum TMR ratio with a 1.26 nm uniform Al layer oxidized for 40, 60, 90, and 120 s. Averaged phase shift profiles perpendicular to the barrier layer in MTJs with (**b**) over-, (**c**) optimum-, and (**d**) underoxidized barriers (Reprinted with permission from [33]. Copyright (2003), AIP Publishing LLC) [32, 33]

Types of Al–O Based MTJs

Sandwich-Structured MTJ

As mentioned above, sandwich structure (F/I/F) is essential for MTJ. In this structure, the coercivities of top and bottom ferromagnetic layers are usually designed to be different. Under an external magnetic field, the layer with smaller coercivity will flip first, thus generating the antiparallel configuration of magnetic moment and two resistance states can be formed.

In sandwich structure, the magnetic moment direction of the two FM electrodes is not "fixed," and so its thermo-stability and the magnetic anti-interference ability is poor for applications. This sandwich structure is difficult to be used as the field-driven magnetic sensor unit or MRAM due to the lack of one-to-one correspondence between MR and applied external magnetic field. However, these sandwich structured MTJs have another practical device application in which the

magnetization can be switched by spin polarization current. Han et al. [41] prepared nano-MTJs based on sandwich structure, and realized the current induced magnetization switching. They observed the relation curve between MR and spin polarized current (R~I), which can be used in on-off type magnetic sensor or MRAM. Moreover, current induced magnetization switching in perpendicular sandwich structured MTJs was also observed [42]. The sandwich structure has many advantages such as easy to prepare and optimize by heating process because of the absence of antiferromagnetic pinning layer. Therefore, the diffusion of Mn atom in normally used antiferromagnetic pinned layer can be avoided. This will result in relatively higher MR in this kind of MTJs.

Spin-Valve Type Pinned MTJ

To overcome the weak thermo-stability and magnetic anti-interference ability in sandwich structure, Dieny et al. [43] designed the pinned spin-valve MTJ in 1991 which brought a breakthrough in application of MR structure. The spin valve magnetic multilayer is comprised of [antiferromagnetic layer/ferromagnetic layer (pinned layer)/non-magnetic metal layer or barrier layer/ferromagnetic layer (free layer)]. After the discovery of MR effect at room temperature, the spin valve structures are widely used in MTJs. In order to improve the stability of pinned FM electrode, artificial AFM coupled structure [AFM/FM/NM metal/FM (pinned)/barrier/FM (free)] is normally used. The main advantage of spin valve pinned structure is the improved sensitivity of free layer to small external magnetic field. Moreover, FM electrode is pinned by antiferromagnetic layers producing the better thermo-stability and magnetic anti-interference ability. There is also a good correspondence between MR and applied external magnetic field, which meet the requirement for device application.

Double Barrier Magnetic Tunnel Junction (DBMTJ)

The typical structure of double barrier magnetic tunnel junctions (DBMTJs) [9–11, 44–48] consists of AFM/FM/I/FM/I/FM/AFM multilayer. The magnetic moment of top and bottom FM electrodes are “pinned” by AFM. The middle FM layer is free, and it is sandwiched between two insulator layers. The quantum well and the resonant tunneling of spin carriers can be formed in the middle layer giving rise to the rich physical properties of DBMTJs structure. Figure 5 shows the typical M-H and R-H curves [44]; three features of loop can be observed which correspond to three arrangements of magnetic moment of three FM layers. Low resistance state can be achieved when the magnetic moment of all three FM layers are parallel, whereas high resistance state corresponds to the antiparallel alignment between the free layer and the two pinned layers. However, when the magnetization direction of the free layer is parallel to the top pinned FM layer but antiparallel to the bottom pinned FM layer, it shows the intermediate state.

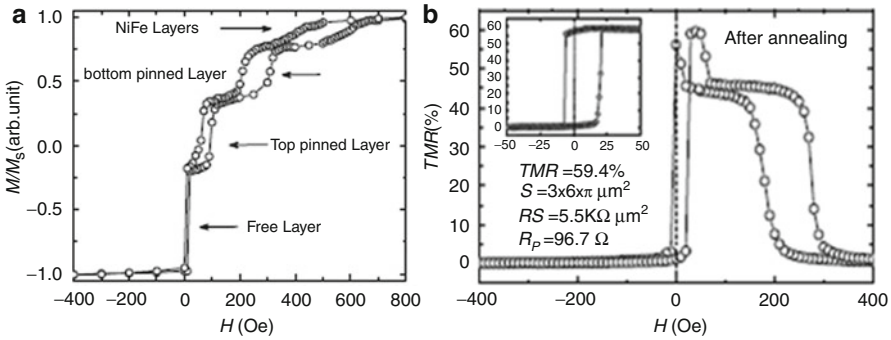

Fig. 5 Magnetization loop (**a**), and TMR major curves and minor loop (*inset*) (**b**) measured at RT for a typical DBMTJ after annealing at 275 °C for an hour (Reprinted from [44]. Copyright (2006) with permission from Elsevier)

Half-Metal MTJ

The half-metallic materials show 100 % spin polarization at Fermi energy, and so high MR can be expected if they are used as FM electrodes. In 1997, Tanaka et al. [49] initiated the research on Al–O based MTJs with half-metal electrodes. In 2003, Inomata et al. [50] achieved 16 % MR using half-metal $Co_2Cr_{0.6}Fe_{0.4}Al$ (CCFA) as FM electrode in Al–O based MTJ (Fig. 6). Recently, Al–O and Mg–O based MTJs with half-metal electrodes have attracted great research interests [51].

Perpendicular Anisotropic MTJ

In perpendicular anisotropic MTJs (p-MTJ), perpendicular anisotropic materials are used as FM electrode. The thermal stability can be enhanced in this kind of MTJ. Perpendicular anisotropy material based MTJs reduces the critical spin polarized current density for magnetization switching. They are useful to reduce the power consumption of device and show a good compatibility with semiconductor technology. Since the year 2000, the research on perpendicular anisotropy Al–O based MTJ has been reported [52–54]. In 2002, GdFeCo(50 nm)/CoFe/Al_2O_3(2.2 nm)/CoFe/TbFeCo(30 nm) based MTJs were prepared by Nishimura et al. [53] and 50 % MR ratio was obtained at room temperature, as shown in Fig. 7.

However, the TMR ratio of perpendicular anisotropy MTJs is smaller than that of in-plane anisotropy MTJs because the spin polarization of perpendicular anisotropy FM thin-film material has relatively small spin-polarization at the barrier interface, and the spin orbit coupling effect enhances the spin scattering effects.

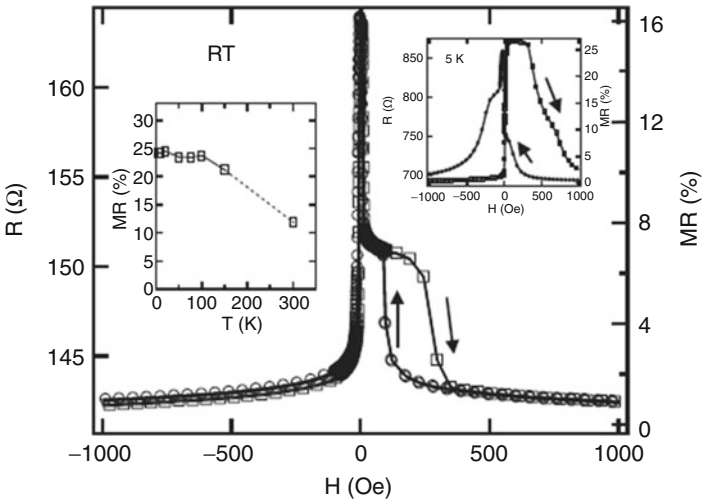

Fig. 6 Magnetoresistance curve at RT for a spin-valve-type magnetic tunneling junction consisting of CCFA(10 nm)/AlO_x(1.8 nm)/CoFe(3 nm)/NiFe(5 nm)/IrMn(15 nm)/Ta(10 nm) fabricated on a thermally oxidized Si substrate at RT. The *upper right inset* shows TMR curve at 5 K, exhibiting 26.5 % TMR. *Inset* on the *left-hand side* is the temperature dependence of the TMR for another sample with the same layer structure [50] (Copyright (2003) The Japan Society of Applied Physics)

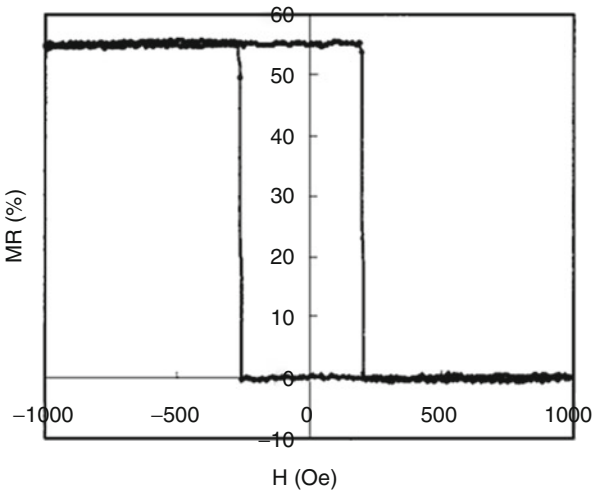

Fig. 7 Tunneling magnetoresistance curve measured at RT for GdFeCo (50 nm)/CoFe/Al_2O_3(2.2 nm)/CoFe/TbFeCo(30 nm) as deposited ($RA = 6.5 \times 10^6$ $\Omega\mu m^2$) (Reprinted with permission from [53]. Copyright (2002), AIP Publishing LLC)

Dilute Magnetic Semiconductors Composite MTJ

Semiconductors are the basic materials in world's electronics industry and have been studied for almost a century. In the past, the semiconductor material was used in electronics based on the control of charge of the carriers without using the spin degree.

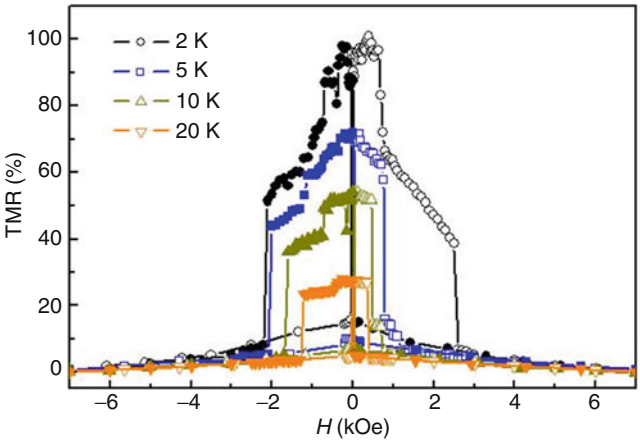

Fig. 8 Magnetic field dependence of TMR ratio at temperatures of 2, 5, 10, and 20 K. The *closed symbols* and *open symbols* represent the field from 7 kOe to −7 kOe and from −7 kOe to 7 kOe, respectively (Reprinted with permission from [55]. Copyright (2011), AIP Publishing LLC)

If both the charge and spin can be controlled in semiconductors, the storage, logical operation, and information communication in one material can be manipulated, resulting in huge economic benefits. Freedom of spin degree in semiconductors can be applied and/or observed by doping with transition metal.

Until now, many works about different kinds of magnetic semiconductors have been reported. A ferromagnetic semiconductor (Ga,Mn)As with Curie temperature T_C as high as 110 K was first prepared using LT-MBE and reported in 1996 by H. Ohno [6], later (Ga,Mn)As was extensively studied. Han and Zhao research groups cooperatively reported the fabrication of MTJ based on (Ga,Mn)As/AlO_x/CoFeB hybrid structures [7]. Their results showed that junction resistance and TMR ratio decreases rapidly with increasing sense current. However, the TMR ratio in this structure is relatively small; the reason is that (Ga,Mn)As surface was oxidized, which reduced the spin injection from CoFeB electrode in Al–O barrier layer. Han and Zhao [55] have also used annealing and plasma cleaning method to reduce and/or remove the surface oxidation thus achieving successfully the TMR ratio as high as 101 % at 2 K in FM/semiconductor hybrid MTJ: $Co_{40}Fe_{40}B_{20}/AlO_x$/(Ga, Mn)As. This is the largest TMR ratio reported in Al–O based FM/semiconductor hybrid MTJs until now (Fig. 8).

Superconductors Composite MTJ

MTJs can be applied in magnetic read head, magnetic sensors, MRAM, STNO, and in the probe of physical interaction, e.g., the influence of superconductivity on magnetism. For a long time, people had great interest in the study of interplay between magnet and superconductor. When the ferromagnetic and superconducting

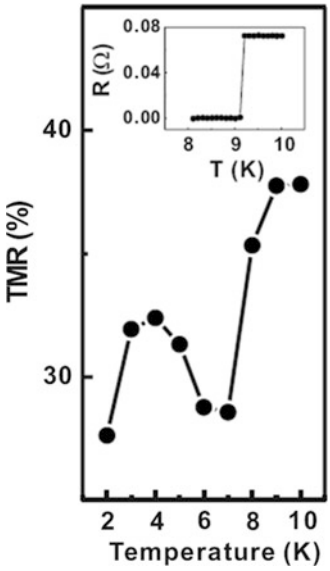

Fig. 9 The plot of TMR ratio with respect to temperature for the S/MTJ sample with $t_{Nb} = 240$ nm. *Inset* indicates the resistance variation of the Nb overlayer in the neighborhood of the superconducting phase transition ($Tc = 9.16$ K) (Reprinted with permission from [7]. Copyright (2009) by the American Physical Society)

materials are brought closer to each other, the FM material may produce strong influence on superconductor because the interior exchange field in FM material can break the superconductive order. Jiang et al. [56] found that Curie temperature of superconducting film oscillates with the thickness of FM layer, in Nb(3)/(Gd(d_{Gd})/Nb(d_{Nb}))$_N$/Gd(d_{Gd})/Nb(3 nm) multilayer. However, in Ni(7)/Nb(d_s)/Ni(7)/FeMn(8)/Nb(2 nm) structure, the Curie temperature of superconducting film show big difference when the magnetizations of the FM layers are parallel or antiparallel [57]. One will ask, "since ferromagnetism can influence the behavior of superconductor, so can superconductivity generate influence to ferromagnetism?" The answer is yes. Although some theoretical works indicated that the superconducting coherence length (ε_F) is very short in ferromagnetic material, however, experiments have already proved that the depth superconducting state function is longer than ε_F [58, 59]. Recently, some experimental work reported that the superconductivity can even change the magnetic properties of adjacent ferromagnetic layers [60–62]. In 2009, Y. M. Chang et al. [8] combined superconductor with free layer of MTJs. Chang et al. utilized practically the proximity effect by bringing superconductor in contact with the free layer in the structure: Nb(t)/CoFe(30)/Al–O(2.5)/CoFe(15)/NiFe(10 nm) [8] (Fig. 9).

Granular Film Composite MTJ

The core structure of granular composite MTJ consists of top FM electrode, barrier layer, and bottom FM electrode. However, the barrier is fabricated by an insulating layer embedded with nano-particles. When the size of magnetic metal particles is in

nanometer range, the electron transport is not only spin-dependent but also exhibits single electron charging effect due to the Coulomb blockade. Prominent TMR effect may arise in these composite MTJs.

Before the discovery of TMR effect in MTJs, in 1972 Gittleman et al. observed the magneto resistance in Ni–Si–O granular film [63]. In 1976, Helman and Abeles also observed the magneto resistance in the same structure, and they indicated the tunneling behavior between particles [64]. In 1995, Fujimori et al. observed 10 % (20 %) MR at room (low) temperature in Co–Al–O granular film, and started the research upsurge about granular films composite MTJs. Co–Al–O granular films became an important research topic, and the transport properties were investigated. Experiments confirmed that the electrons tunnel through Al–O barrier between Co particles [65].

In the magnetic granular film, the metal particles are separated by insulating medium, and electrons tunnel between metal particles. This tunneling process involves several particles, sometimes, the transport of electrons need multiple tunneling between the metal particle and its neighbor particles. For multiple tunneling processes, there are two possible transport mechanisms: sequential tunneling [66] and co-tunneling [67]. Sequential tunneling model implicates that the tunneling of electrons is successive; while co-tunneling considers that if one electron tunnels into one particle, another electron tunnels out form this particle at the same time. When the particle size is small enough, the number of electrons increased in particles will improve electrostatic energy of particles; when the energy is bigger than bias and thermal disturbance, the tunneling process will be inhibited and Coulomb blockade effect appears. The particle energy will increase during every tunneling process in sequential tunneling, but the energy of system will not increase in co-tunneling process. In early research on single-electron transistor, people demonstrated that sequential tunneling will be suppressed and co-tunneling process contribute to the electron transport. It can be deduced that tunneling probability is large in the case of high temperature or high bias. Takahashi et al. proved theoretically the co-tunneling between particles will result in increased value of MR [68]. Experimentally, both sequential tunneling and co-tunneling are found to exist in insulated granular films [65, 69].

Nano-Ring-Shaped MTJ

Solid rectangular or elliptical-shaped MTJs are usually used as the core unit in conventional MTJs based magnetic sensors, MRAM, and spin nano-oscillators, etc., due to the shape anisotropy that can be used to increase the thermal stability of the device. However, there is stray field appearing along the edge of the long axis in rectangular or elliptical-shape MTJs. Especially, when the unit size and separation distance in arrays become small, the stray field between free layer, reference layer, and adjacent units will significantly increase. This increased stray field will induce magnetic interference and magnetic noise which has a serious affect on the device performance by limiting the increase of density of units. For nano-ring and

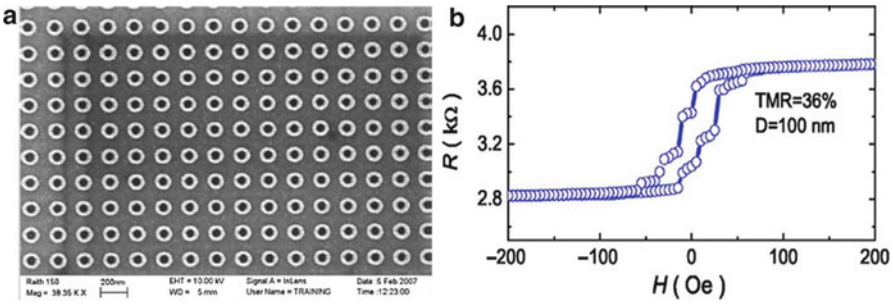

Fig. 10 (**a**) Scanning electron micrographs (SEMs) of nanoring MTJ arrays with outer diameter $D = 100$ nm and ring width (W) narrower than 30 nm. (**b**) Resistance versus magnetic field loops for NR-MTJ sample with $D = 100$ nm, the temperature is 300 K (Reprinted with permission from [134]. Copyright (2007), AIP Publishing LLC)

nano-elliptical ring MTJs, free layer and reference layer were patterned into closed circular ring by nanofabrication. As a result, closed magnetic moment will be formed. This closed magnetic domain does not produce stray magnetic fields, and the inter-coupling interference does not exist in adjacent storage units. Because of its closed shape, nano-ring or nano-elliptical ring MTJs have better thermal stability. In addition, it will eliminate demagnetizing field in two open ends in the rectangular or ellipse-shaped nano-MTJs, so the critical switching current density can be decreased in this structure.

Han's group [41, 134] designed nano-ring MTJs by growing Ta(5 nm)/Ru(10)/Ta(5)/$Ni_{81}Fe_{19}$(5)/$Ir_{22}Mn_{78}$(12)/CoFe(2)/Ru(0.9)/CoFeB(3)/Al(0.6-Oxide)/CoFeB(2.5)/Ta(5)/Ru(6) multi-layers on Si(100)/SiO_2 substrate using magnetic sputtering method. Micro-nano processing was used to pattern nano-ring MTJs. They successfully prepared nano-ring MTJs with outer diameter of 100 nm and width of about 25 nm [41, 134]. Figure 10 shows the R-H curves of NR-MTJ which show that the resistance is 2.8 kΩ (3.8 kΩ) when magnetic moment aligned parallel (antiparallel), and the resulting TMR ratio is 36 % at room temperature.

Quantum Effects and Magnetoelectric Properties of Al–O Based MTJ

Temperature and Bias Dependence of Magnetoresistance Effect

The tunnel magneto-resistance rely on the ferromagnetic electrodes, tunnel barrier, and interface, especially its strong dependence on the temperature and bias. In most of the cases, the TMR and tunnel resistance decreases with increase in temperature. Shang and Moodera et al. [70, 71] suggested a spin-wave excitation model to explain this phenomenon. They suppose that with the increase of temperature, spin polarization P of magnetic electrodes obey the Bloch law which is given as $P(T) = P(0)(1-\alpha T^{3/2})$. MacDonald [72] considered the variation of quasi-particles'

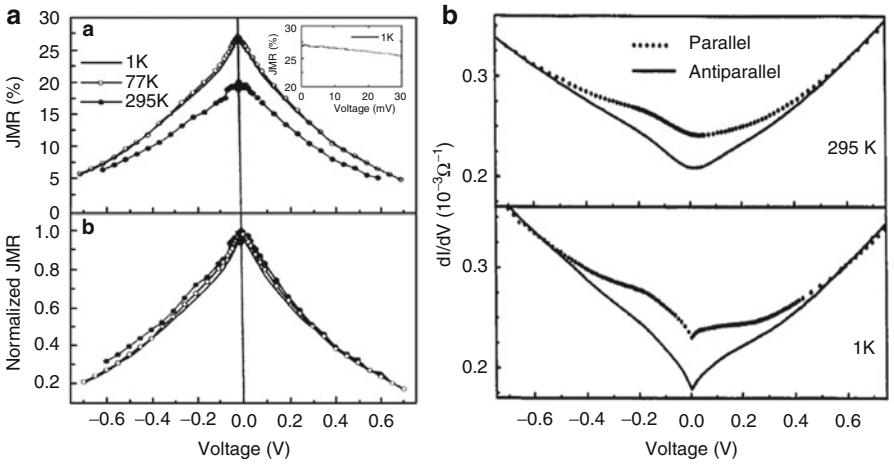

Fig. 11 (**a**) The bias dependence curve of TMR and (**b**) conductance at different temperatures in $Co/Al_2O_3/Ni_{80}Fe_{20}$ (Reprinted with permission from [70]. Copyright (1998) by the American Physical Society)

spectral weight function with temperature to prove that the spin polarization and saturation magnetization have the same temperature relation, i.e., P(T)/P(0) = M(T)/M(0) and $TMR(T) = TMR(\mathrm{T} = 0)(1-\mathrm{A}T^{3/2} + \ldots)$. This model has been successfully applied to MTJs composed of different electrodes and barriers [73–75].

Besides the spin-wave excitation model, inelastic scattering mechanism can also result in the decrease of TMR with the increase in temperature. For example, Zhang et al. [76] proposed the interfacial magnon assisted tunneling process and explained the bias and temperature dependence of TMR; their model agrees well with the experiments. Bratkovsky [77, 78] take into account the magnon, phonon, and impurity scattering on equal footing to explain the temperature and bias dependence. Vedyayev emphasizes the role of spin-flip scattering caused by magnetic impurities in barrier [79]. The number of spin-flip electrons will increase with the temperature, causing the reduction of TMR ratio.

MTJs are a kind of non-linear elements. The bias dependence in parallel and antiparallel states shows different behavior. The bias dependence behavior of MTJs is closely relevant to performance of spintronic devices and thus its bias properties are not only important for the fundamental research but are also crucial from application point of view. The TMR of almost all of the Al–O MTJs are found to decrease with increasing values of bias voltage. The voltage at which the TMR drops to half of its maximum value is termed V_{half}. It is an important parameter to evaluate the quality of MTJs. Usually, for the device application, it is better to have larger value of V_{half}. The $V_{1/2}$ of about 200 mV [3, 71] was found in the early experiments. Figure 11 shows the (a) bias dependence curve of TMR and (b) tunnel conductance. The TMR decreases with the increase of bias voltage and zero bias anomaly can also be observed in such cases. Recently, the $V_{1/2}$ value achieved by some groups exceeded 500 mV [80–82].

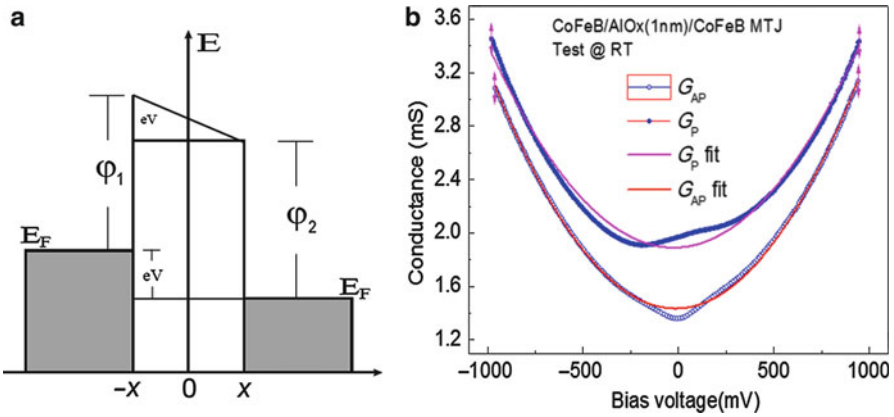

Fig. 12 (**a**) The energy band of MTJs under bias voltage. (**b**) The bias dependence of G_P *and* G_{AP} in CoFeB/Al–O/CoFeB MTJs. The *solid lines* are the fitted results [83]

In tunnel junctions, free electron models are usually used to describe the conductance bias dependence. One of the most widely used models is Simmons' tunneling model. In this model, the WKB approximation was used and the interaction between electrons was neglected. When $T = 0$K and $V << \varphi$, the bias dependence of conductance can be simplified into the following quadratic form:

$$G(V) = G_0\left[1 - 2C_1\frac{s\Delta\varphi}{\overline{\varphi}^{3/2}}V + 3C_2\frac{s^2}{\overline{\varphi}}V^2\right] \tag{1}$$

where, $\overline{\varphi} = (\varphi_1 + \varphi_2)/2, \Delta\varphi = \varphi_1 - \varphi_2, G_0 = C_3\frac{\sqrt{\varphi}}{s}\exp(-1.025s\sqrt{\overline{\varphi}})$, C_1, C_2, and C_3 are constants: $C_1 = 0.0854\ \mathrm{m^{-1}V^{-3/2}}, C_2 = 0.0984\ \mathrm{m^{-2}V^{-2}}, C_3 = 31.6\ \mathrm{nm^{-1}V^{-3/2}}$. By fitting the equation, the effective height (φ), width (d) as well as the potential difference of barrier ($\varphi_1 - \varphi_2$) can be obtained.

Figure 12 is the fitting results for typical Al–O MTJs: IrMn(12)/CoFe(2)/Ru (0.85)/CoFeB(3) /Al–O(1)/CoFeB(4 nm). The effective barrier thickness is 0.9 nm, the effective barrier height for parallel and antiparallel state are 2.17 eV and 2.76 eV, respectively.

Following are some main features of the G-V curves: (1) both, parallel and antiparallel conductances increase by increasing the voltage, (2) the antiparallel conductance increases more quickly than the parallel conductance, resulting in the decrease of TMR, especially in the range of ±200 meV. Zhang et al. [76] proposed a model suggesting that inelastic scattering by magnon excitations at the ferromagnet/insulator interface controls the voltage dependence. In the presence of bias, tunnel electrons with energies above the Fermi level, known as "hot electrons," may tunnel by emitting a magnon. With increase in the bias voltage, more magnons can be emitted, resulting in the increased conductance and reduced TMR values. This model is able to reproduce the zero bias anomalies in conductance and MR of

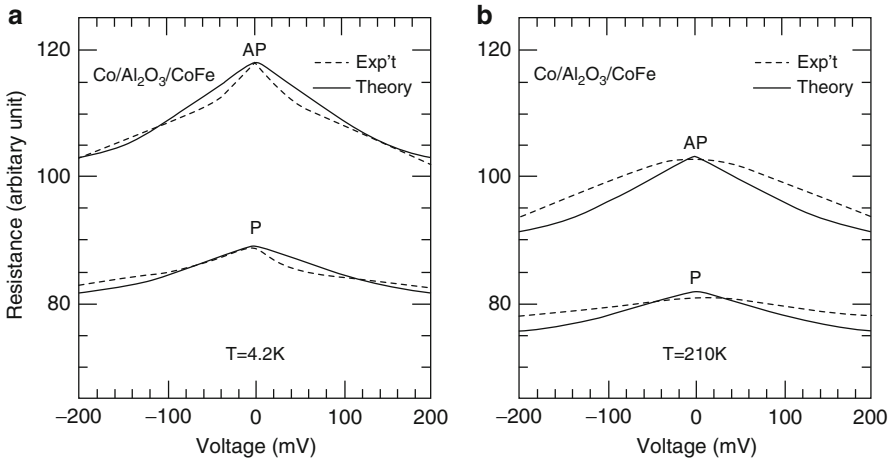

Fig. 13 Resistance as a function of bias voltage for P and AP states in $Co/Al_2O_3/CoFe$ at two different temperatures: (**a**) T = 4.2 K and (**b**) T = 210 K. The *dashed lines* are experimental data; *solid lines* are theoretical results (Reprinted with permission from [76]. Copyright (1997) by the American Physical Society)

MTJs. This model was used by Han et al. [84] who performed a careful analysis of the conductance and MR as a function of voltage and temperature for $Co_{75}Fe_{25}/Al_2O_3/Co_{75}Fe_{25}$ tunnel junctions. They also found that when the magnetizations of electrodes are in different alignments, the cutoff energy of interface magnons is anisotropic. The experimental data was better fitted by considering this anisotropic cutoff energy. Later, the phonons contribution was added by Wu et al. [85]. Bratkovsky et al. suggested the inclusion of the phonon and impurity assisted process at high bias voltage [77, 78] (Fig. 13).

Magnon excitations are the main mechanism to investigate the bias properties. However, in some special cases, other mechanisms, for example, the phonon scattering by impurities, contribute as well [86–89]. Besides the contribution from the inelastic tunneling, Davis et al., pointed out that the variation of electron interface density of states is also an important factor for the bias dependence of TMR [90–93].

Inelastic Electron Tunneling Spectroscopy (IETS) of MTJ

IETS is a powerful tool to investigate the inelastic tunneling process in MTJs, for example, it helps in determining which excitation process plays a role in tunneling. Moreover, density of the excitation will also be reflected from the IETS. Figure 14 shows different types of IETS corresponding to paramagnetic impurity, magnons, and phonons. When paramagnetic impurities are present in the junctions, the conductance will decrease with the increase of bias near the zero bias. Thus, a

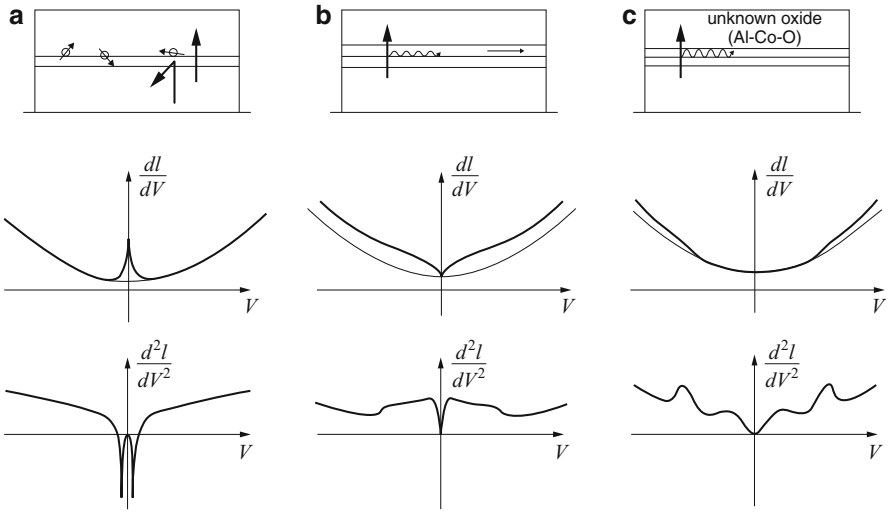

Fig. 14 The schematic illustrations of three type of IETS by: (**a**) impurity, (**b**) magnon, and (**c**) phonon [94]

negative peak will appear in the IETS. When there are magnons or phonons, additional scattering path will be opened and there will be positive peaks in IETS. The relevant peak position reflects the magnons or phonons density of states [94].

Moodera group found two main peaks appearing in TMR (V) curves in $Co/Al_2O_3/Ni_{80}Fe_{20}$ MTJ. One of the peaks was located at 110 mV, visible at all temperatures and the other one was located at 17 mV, only visible at liquid helium temperature (as shown in Fig. 15). Both peaks were originated from the magnon excitation. At the same time, in non-magnetic Al/Al–O/Al junction, Al–O phonon peak can be found at around 100 mV.

Miyazaki's group also observed a peak at 1.2 mV for parallel and antiparallel states in Co/Al–O/Co MTJs. In order to obtain the magnetic contribution, the authors subtracted the IETS data for different states [95]. In CoFe/Al–O/CoFe MTJs [84], they also observed peaks at 5.86 ± 1.0 mV for parallel and 19.5 ± 1.0 mV for antiparallel at 4.2 K. In the low bias regime (lower than 200 mV), most research groups reached the same conclusions: the value of IETS for antiparallel alignment should be larger than for parallel alignment. In Al–O MTJs, the information of phonon can also be traced from the IETS. The peaks in IETS that are arising from the phonons should have the same position, magnitude, and half width for the two alignments, as shown in Fig. 16.

On the other hand, very sharp peaks in the IETS of magnetic tunnel junctions at low bias closely resemble the derivative of the so-called zero-bias anomaly of nonmagnetic tunnel junctions which is attributed to magnetic impurity scattering rather than the magnon scattering mechanism [76, 96–98]. Wei et al. [99] performed a series of systematic measurements in several different types of

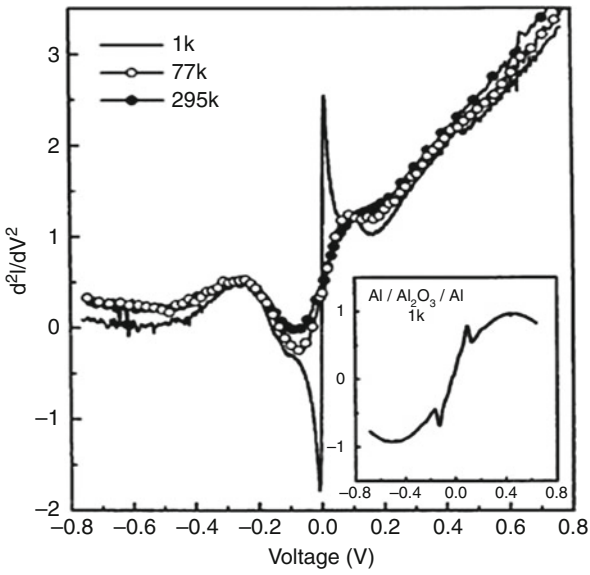

Fig. 15 IETS of $Co/Al_2O_3/Ni_{80}Fe_{20}$ MTJ at different temperatures. The *inset* shows the IETS of Al/Al–O/Al at T = 1 K (Reprinted with permission from [70]. Copyright (1998) by the American Physical Society)

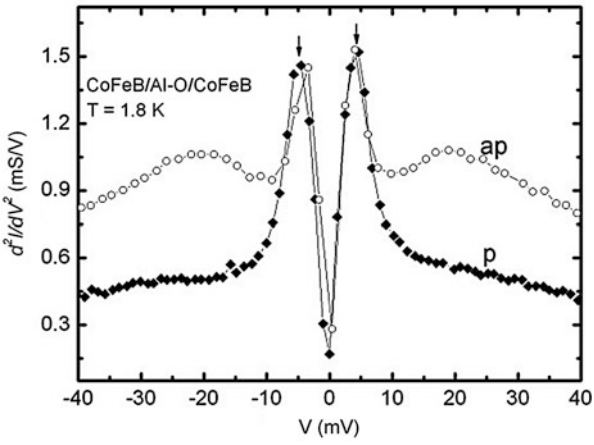

Fig. 16 IETS of CoFeB/Al–O/CoFeB MTJs at T = 1.8 K; peaks at ±4 mV are originated from phonon excitation and peaks at ±20 mV arise due to the magnon excitation [83]

MTJs. The measurements show that both types of scattering exist in all junctions. The behavior attributed to magnetic impurity and magnon scattering show differences in the IETS. At low temperatures, it produces an IETS pattern consisting of three flat plateaus with discontinuities at $eV = \pm Ec$, where Ec is the magnon activation energy. Magnetic impurity scattering produces a logarithmic singularity in the conductance which corresponds to two very sharp peaks near zero bias in the IETS. In particular, in the antiparallel configuration scattering is dominated by interface magnon scattering but magnetic impurity scattering is clearly visible in the IETS. The authors withdraw some of the approximations and include both

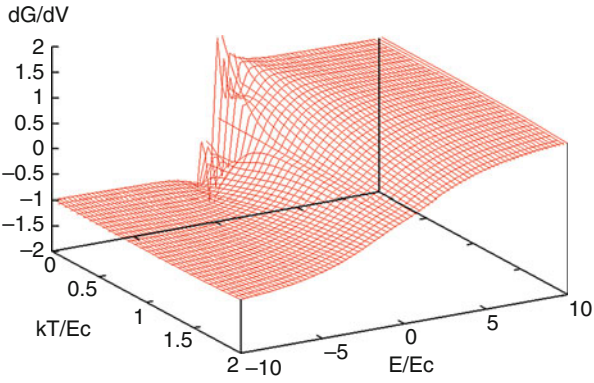

Fig. 17 dG_{magnon}/dV as a function of E/Ec and kT/Ec, with both the contributions, i.e., surface magnon and magnetic impurity contribution (Reprinted with permission from [99]. Copyright (2010) by the American Physical Society)

magnon scattering and magnetic impurity scattering mechanisms. For example, the contribution of magnetic impurity to the conductance is:

$$G_{\text{impurity}} = G_2 - G_3\left[F(|eV|,T) + \frac{1}{2}F(|eV+\Delta|,T) + \frac{1}{2}F(|eV-\Delta|,T)\right] \quad (2)$$

where, G_2 is the conductance due to the second-order tunneling process and can be viewed as a background conductance, and the G_3F term is the third-order term that yields the zero bias anomaly. Δ measures the exchange coupling strength between the impurities and the electrodes.

The magnon contribution to the conductance is:

$$G_{\text{magnon}} = C\left\{-2kT\ln\left[1-e^{-E_C/kT}\right] + \frac{|eV|+E_C}{e^{(|eV|+E_C)/kT}-1} + \frac{|eV|-E_C}{1-e^{-(|eV|-E_C)/kT}}\right\} \quad (3)$$

where, E_C is the lower cutoffs for the magnon energy.

From the analytical solution of the magnon scattering model, the authors found that surface magnon scattering alone does not give rise to sharp peaks in the IETS. Instead, the magnetic impurity coupled to the magnetic electrodes produced the observed two peaks Fig. 17. The above model can be generated to include the phonon contribution.

Quantum Well Effect in Al–O Based MTJ

Spin-polarized resonant tunneling is the fundamental physical mechanism which is necessary for the development of highly functional devices such as spin transistors, etc. [100]. One of the simplest ways to realize spin-polarized resonant tunneling is to insert a nonmagnetic (NM) metal layer between the insulating tunnel barrier (I) and one of the two FM electrodes in an MTJ as shown in Fig. 18. Spin-dependent reflections of the conduction electrons take place at the

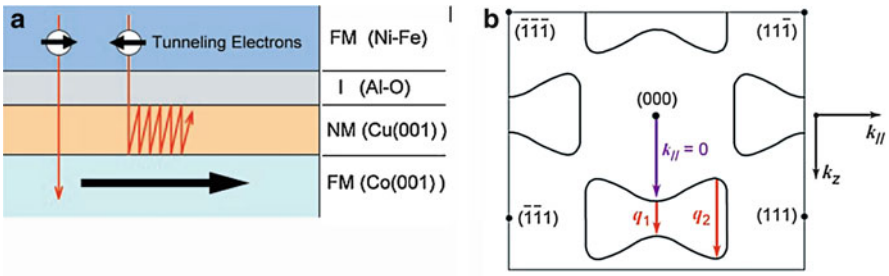

Fig. 18 (**a**) Schematic diagram of Co(001)/Cu(001)/Al–O/NiFe MTJs. (**b**) Fermi surface of fcc-Cu, when conduction electrons are confined in the [001]-direction, quantum well states with scattering vectors $\mathbf{q}_1$ and $\mathbf{q}_2$ can be created (From [106]. Reprinted with permission from AAAS)

FM-NM interface (Fig. 1A) thus creating spin-polarized quantum well (QW) states in the NM layer [101, 102] and spin-polarized tunneling electrons will resonantly pass through the NM layer. To date, the TMR ratio is usually found to decrease monotonically with NM layer thickness. Although, a number of experimental studies have been done, there are no reports on TMR oscillation being observed by many researchers [103–105]. This can be attributed to the short electron mean free path in poly-crystalline samples. In 2002, high quality Co(001)/Cu(001)/Al–O/NiFe-MTJs have been fabricated by MBE by Yuasa et al. and a clear oscillatory MR as a function of Cu thickness was observed [106]. The bottom electrode Co(001)/Cu(001) is single crystal, Al–O is an amorphous barrier, and the top NiFe electrode is poly-crystalline. As shown in the schematic diagram in Fig. 18a, when two electrodes are in parallel alignment, the majority electrons in NiFe electrodes tunnel across the junction and the minority electrodes will be reflected back and forth at Cu/Co and AlO_x/Cu interfaces. Consequently, the quantum well states will be created in Cu. The energy band calculation for fcc-Cu shown there are $\mathbf{q}_1$ and $\mathbf{q}_2$ scattering vectors which will produce two periods 10.6 Å and 5.9 Å.

As shown in Fig. 19c, at T = 2 K and T = 300 K, the TMR shows obvious oscillation as a function of Cu thickness. In some thickness range, the TMR oscillate between positive and negative value. Figure 19a, b shows the MR curve corresponding to the Cu thicknesses of 0 Å and 4.5 Å, respectively. The MR is positive and remains normal when the thickness of Cu is 0 Å, while, the MR becomes negative when the thickness of Cu is 4.5 Å. The fitted oscillation period is 11.4 Å which corresponds to the long period oscillation from the $\mathbf{q}_1$ vector. The period of exchange coupling in Co(001)/Cu(001)/Co(001) structure, fabricated by the same method, is also 11 Å. This proves that the oscillations arise from the same $\mathbf{q}_1$ vector. In single crystalline MgO MTJs,the tunneling is coherent, thus the MR oscillation caused by the insertion of non-magnetic layers will be easier to be observed experimentally [107, 108] and the first-principles calculations can be employed in order to clearly reveal the physical mechanism behind it [109, 110].

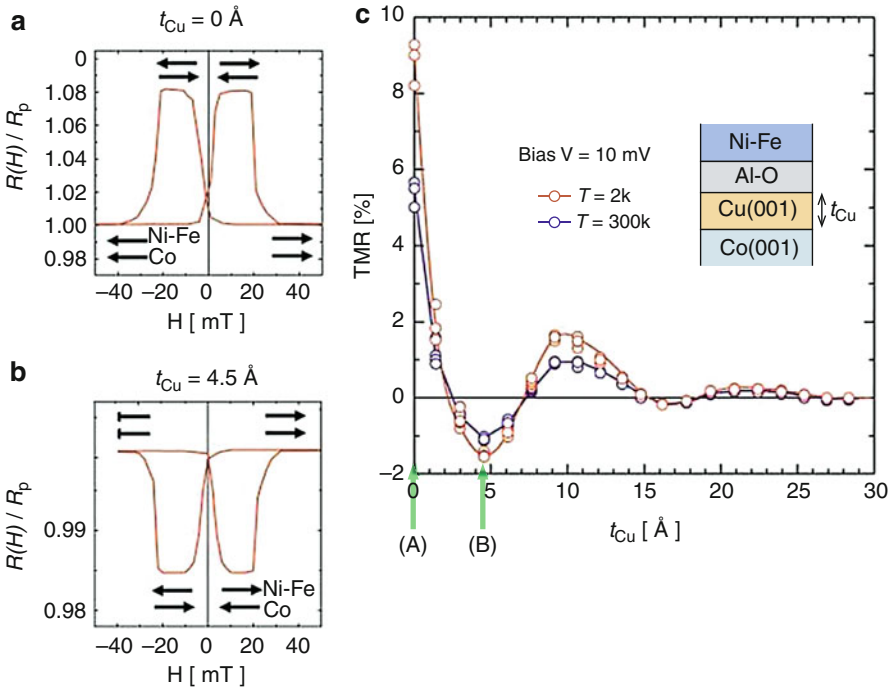

Fig. 19 At 10 mV bias, normalized TMR at $T = 2$ K in Co(001)/Cu(001)/Al–O(18 Å)/ $Ni_{80}Fe_{20}$ MTJs with different Cu thickness: (**a**) 0 Å and (**b**) 4.5 Å (**c**). The TMR oscillates as a function of Cu thickness at two different temperature: $T = 2$ K and 300 K (From [106]. Reprinted with permission from AAAS)

Magnetoresistance Oscillation Effect in MTJ

Double barrier magnetic tunnel junctions (DBMTJs) have drawn much research attention due to its rich physics and promising applications in spintronic devices. In 1997, Zhang et al. [105, 111, 112] used Slonczwski free electron model and transfer matrix method to calculate the bias dependence of TMR in FM/I/FM/I/FM DBMTJ. Their results show the tunnel conductance and TMR oscillation as a function of bias voltage. Sheng et al., [9] used Landauer Büttiker scattering method to study the transport properties in DBMTJs and found the non-linear dependence of TMR on bias voltage. Barnas et al. [113, 114] observed the MR oscillation due to the charge effect in the middle magnetic layers. Later, Vedyayev et al. [115, 116] generated the DBMTJ model to multiply DBMTJs and a pronounced oscillation was predicted.

One year after the predictions, a series of experimental progress was done. In 1998, Montaigne et al. [10] first reported the measurement of MR effect in $Co/AlO_x/Co/AlO_x/Ni_{80}Fe_{20}$ DBMTJ. As shown in Fig. 20 (left), the TMR ratio is around 11 % at room temperature which is lower than the value of 16 % in single barrier MTJs. As shown in Fig. 20 (right), in single barrier MTJs, $V_{1/2}$ is around

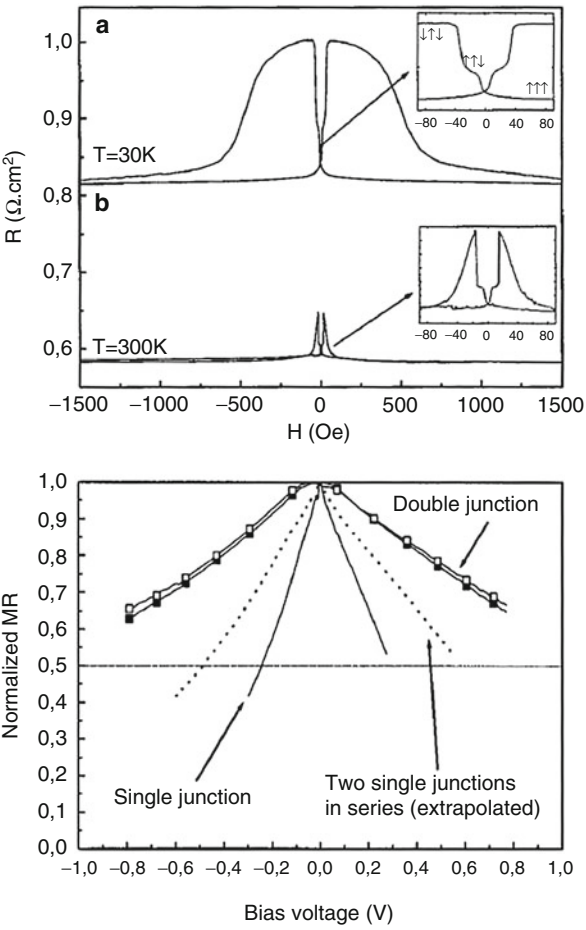

Fig. 20 TMR dependence in DBMTJs on magnetic field (*left*) and bias (*right*) (Reprinted with permission from [10]. Copyright (1998), AIP Publishing LLC)

0.26 V, but in DBMTJ it is larger than 0.8 V. In 2001, Saito et al. [10] investigated the transport properties in IrMn/CoFe/AlO_x/CoFe/AlO_x/CoFe/IrMn structure. TMR reaches to 42.4 % and half-width reaches to 872 mV after annealing at 300 K. In almost all the reports, the TMR reported in DBMTJ is found to be lower than that of single barrier MTJ. Han et al. [46, 47] suggested a possible explanation for this phenomenon by micro-magnetic simulations. They pointed out that when current is applied, the vortex domain wall (butterfly-shaped domain wall) will be present in the middle magnetic layer. As a result, the perfect antiparallel state cannot be achieved, resulting in the reduction of TMR in DBMTJs.

In 2003, Colis et al. [48] fabricated CoFe/AlO_x/CoFe/AlO_x/CoFe-DBMTJ. The TMR ratio was 49.5 % at RT and $V_{1/2}$ was 1.33. Zeng et al. [117] prepared $Co_{75}Fe_{25}$/Al–O/$Co_{75}Fe_{25}$/$Ni_{79}Fe_{21}$/ $Co_{75}Fe_{25}$/Al–O /$Co_{75}Fe_{25}$ DBMTJ. They have observed the TMR ratios of 29.4 % and 41 % at room temperature and at 4.2 K, respectively. The bias dependence of conductance and TMR has also been

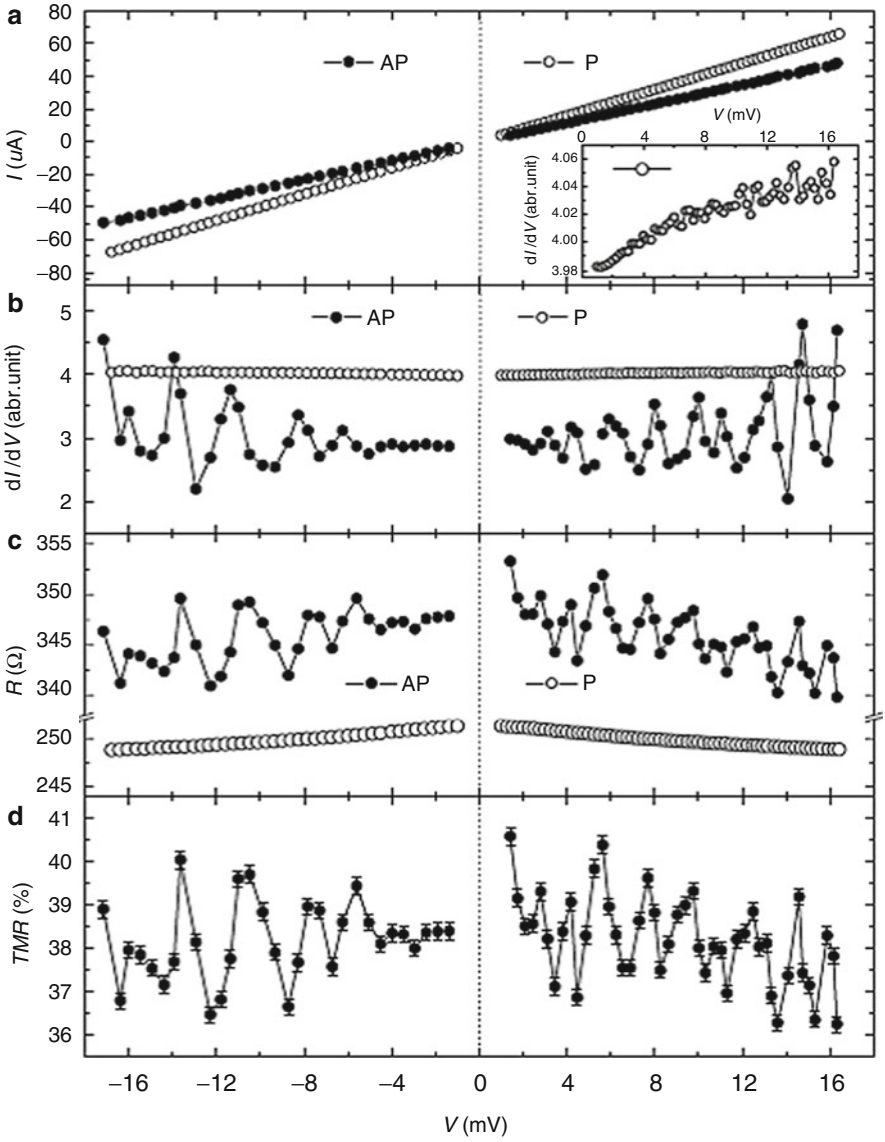

Fig. 21 (**a**) Bias current, (**b**) differential conductance dI /dV, (**c**) tunnel resistance R = V/ I, and (**d**) TMR ratio versus bias voltage curves at 4.2 K for the same patterned DBMTJ (Reprinted with permission from [117]. Copyright (2005) by the American Physical Society)

investigated. As shown in Fig. 21, R_{AP} and TMR show an oscillation with respect to the bias voltage in the AP configuration. On the other hand, there is no visible oscillation in the P configuration. The oscillation of the TMR ratio was attributed to arise from the oscillation of the resistance in AP states. The oscillation period was 1.6 mV.

They proposed that the observed effect may involve additional inelastic scattering mechanisms, more specifically the spin wave emissions in the middle ferromagnetic layer. In a single barrier MTJ, the spin accumulation at the two sides of the electrodes contributes very little to the resistance because the barrier resistance is much larger than the spin accumulation induced resistance [118]. However, an assisted tunneling might occur if the spin accumulation can generate magnons or spin waves in the middle layer because these excitations may assist the electron tunneling from first barrier to the second one. The magnon assisted tunneling has already been investigated in the study of the temperature and voltage dependence of TMR [76, 84]. When the spin accumulation exceeds a critical value, such that the difference of the chemical potentials between spin-up and spin-down channels remains larger than the threshold of the spin wave gap, typically at about 1 meV, magnons can be generated and the magnon-assisted tunneling contributes to the tunnel conductance. In the *P* state, the spin accumulation is parallel to the local moment, and thus the spin wave emission is prohibited by the spin angular momentum conservation, i.e., the magnon-assisted tunneling is suppressed. This mechanism is similar to the current driven spin-wave excitations mechanism suggested by Berger et al. [119].

This research has drawn great interest of the scientific community and further related work is in progress. It is promising that in the future, oscillatory MR can be obtained with high values at the same time.

Spin-Scattering Effect and Spin-Flip Length in MTJ

The FM/I/NM/I/FM DBMTJs can be formed by replacing the middle ferromagnetic metallic (FM) layer with the non-magnetic metals (NM). Zheng [120] and Wilczynski et al. [121] studied the conductance and TMR in this type of DBMTJ at zero bias and finite bias, respectively. Their results show tunneling current at zero bias and TMR oscillations as a function of middle non-magnetic layer thickness. High TMR can be achieved for a particular thickness range, as shown in Fig. 22.

The tunneling process involved here is the coherent tunneling in which the phase of electrons is conserved. There is another tunneling process called “sequential tunneling” that can also occur in DBMTJ. In the sequential tunneling process, the tunneling can be considered to proceed in sequence. The electrons firstly tunnel into the middle layer and then tunnel into the last electrode. In these two processes, electrons lose their phase relation. In the sequential tunneling regime, some theoretical results [122–125] show that the measurable TMR of DBMTJ with NM middle layer is possible only when the electrons have long relaxation time. For coherent tunneling, electrons spend very short time in barrier and thus the spin accumulation effect can be neglected.

One of the challenges in the physics of spin-based electronics, or spintronics, is the study of spin-flip scattering and its effect on magnetotransport, in particular, on spin injection and accumulation. Bratass et al. [123] studied the spin accumulation effect in FM/I/NM/I/FM DBMTJ. TMR is found to be related to the spin

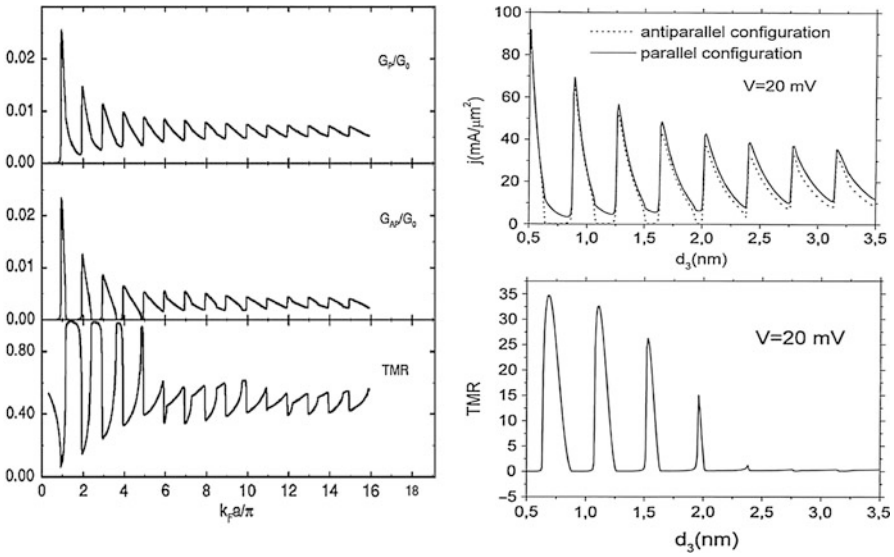

Fig. 22 Conductance and TMR as a function of NM thickness (**a**, Reprinted with permission from [120]. Copyright (1999) by the American Physical Society; **b**, Reprinted from [121]. Copyright (2000) with permission from Elsevier)

accumulation in the middle layer. The TMR effect in DBMTJ can be used to investigate the spin-flip process and to probe the spin-diffusion length in the middle non-magnetic layers. Zeng et al. [124] fabricated CoFe(CoFeB)/AlO/Cu/AlO/CoFe (or CoFeB) DBMTJ with Cu middle layer to investigate the spin-flip scattering. Based on the free-electron model [125], the TMR of DBMTJ can be deduced from the single barrier MTJ:

$$\frac{\Delta R}{R} = \frac{1}{2}\frac{G_P - G_{Ap}}{G_{Ap} + \sqrt{G_P - G_{Ap}}\gamma G_s} \tag{4}$$

where, G_P and G_{AP} are the parallel and antiparallel conductances of SBMTJ, $\gamma^2 = 2R_N$, R_N is the conductance of Cu/Al–O/Cu, and G_s is spin-flip conductance.

Figure 23 shows the bias voltage dependence of γG_s extracted using Eq. (3) from the TMR measurements for CoFeB DBMTJ sample with a Cu spacer layer of 0.5 nm thickness. The nonlinear voltage dependence agrees well with the theory. The bias voltage dependence of γG_s arises directly from the density of states of the Cu layer. The spin-flip conductance γG_s reaches the maximum at about $V = \pm 0.14$ V, when the transport window in the Cu layer reaches the nearest QW. In Fig. 23, γG_s was plotted for two sets of samples as a function of the temperature. For both sets, γG_s increases linearly with the temperature. The slopes of the two lines differ by about a factor of 3, in proportion to the Cu layer thicknesses of 0.5 nm and 1.4 nm for the two DBMTJ samples. The linear temperature dependence and the scaling of the slope with the Cu thickness suggest

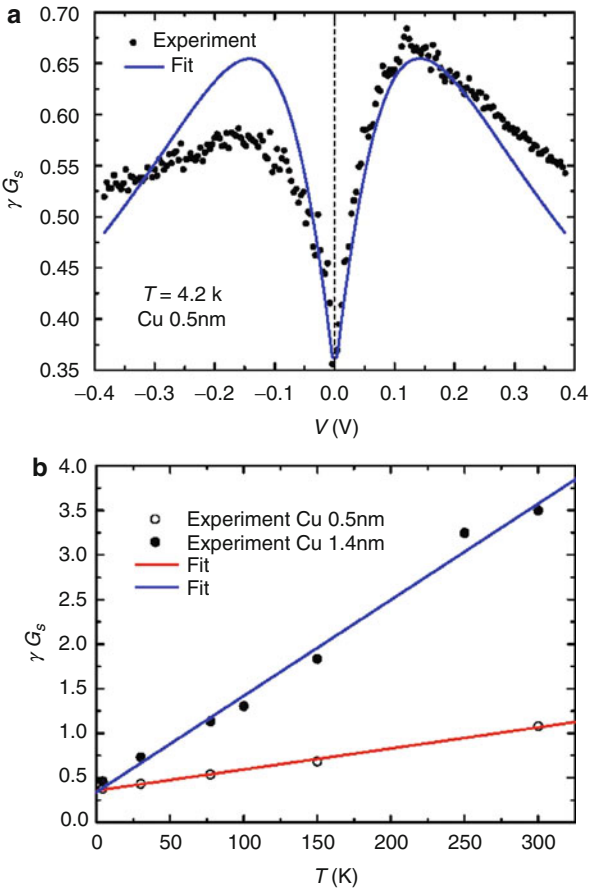

Fig. 23 (**a**) Bias voltage dependence of γGs for the CoFeB DBMTJ sample in comparison with theory (*solid line*). (**b**) Temperature dependence of γGs for CoFe and CoFeB DBMTJ samples (Reprinted with permission from [126]. Copyright (2006) by the American Physical Society)

that the bulk spin-flip scattering may arise from electron–phonon interaction. The room temperature spin-flip length was fitted to be l_{sf} (300 K) = 350 nm [128]. We found that for the Cu = 0.5 nm sample, l_{sf} (4.2 K) = 1.0 μm and for the Cu = 1.4 nm sample, l_{sf} (4.2 K) = 2.6 μm. These values are in agreement with the diffusive regime measurement [128]. This new method can be used to probe the spin diffusion length. It is critical for developing spintronic devices.

Spin-Dependent Coulomb Blockade Magnetoresistance

The spin-dependant phenomenon can be enhanced and novel physics may emerge in this quantum dot or granular system due to the discrete energy level and charge effect. Takanashi et al. [68] studied spin-dependent electron tunneling in ferromagnetic junctions containing small metallic islands. The tunneling matrix elements depend on the relative direction of magnetization of the island and electrodes.

The dependence of the matrix elements amplifies the co-tunneling in the Coulomb blockade regime. They showed that in single-electron ferromagnetic transistors, the MR is strongly enhanced by the Coulomb blockade. Results provide a theoretical basis for recent experiments on ferromagnetic single-electron transistors, ferromagnetic double tunnel junctions, and ferromagnetic granular materials. Barnas et al. [129] used perturbation method to study the transport of MTJs with magnetic nano-dots. Their study shows that in the coulomb blockade regime, the co-tunneling plays a crucial role in the bias dependence of TMR, which results in the zero bias anomalies. In low bias, the TMR is suppressed, indicating that the spin-flip process exists in the barrier. With the increase of bias, spin accumulation reduces the spin-flip process resulting in the gradual increase of TMR. Fettar et al. [130] studied the electric and magnetotransport properties of $Co/Al_2O_3/Co/Al_2O_3/(Co, Cu)$ double tunnel junctions, in which the intermediate Co layer is either granular or percolated clusters and the top electrode is either Co or Cu. In granular junctions, spin-dependent tunneling with Coulomb-blockade effect was observed. The Coulomb blockade effect and the improvement of the antiparallel alignment at low temperature resulted in enhancement of TMR effect.

In 2005, Yakushiji et al. [131] designed Al/Al–O/CoAlO granular/Co/Pt magnetic MTJs as shown in Fig. 24. At low temperature, TMR oscillates as a function of bias. They simulate the bias dependence of TMR with different spin-relaxation time of 1 ns, 10 ns, and 150 ns. By comparing the experiments and simulations, they found that the TMR curve can be best fitted with 150 ns spin-relaxation time. Theoretical analysis of the MR behavior clearly shows that the spin-relaxation time in nanoparticles is highly enhanced in comparison with that in the bulk.

Zhang et al. [12] proposed the spin-dependent Coulomb blockade (CB) voltage as a possible mechanism for producing very large MR. The spin dependence of the CB voltage is realized through the coupling between the QDs due to spin-dependent electron transport, as illustrated in Fig. 25a. As the inter dot conductance is enhanced, the collection of the QDs acts together as a larger QD. This causes a reduction in the CB voltage. When inter dot coupling is controlled by the magnetic moments of the QDs, the Coulomb blockade magnetoresistance (CBMR) effect is produced. The main theoretical formulas are given as follows:

$$\frac{G_H(V)}{G_0(V)} = \frac{(\lambda_0/\lambda_H)^2 \int_{x_V}^{\infty} x^4 F_H(x)dx}{\int_{x_V}^{\infty} x^4 F_0(x)dx} \tag{5}$$

where, λ_H and λ_0 are the effective mean size of nanodots with and without magnetic field, F_H and F_0 are size distribution function of QDs, x_V is the smallest size of QDs which contributed to the conductance under bias V.

The mechanism proposed above is different than the previous considerations of spin-dependent Coulomb blockade effect. In previous models, the Coulomb blockade voltage is assumed to be a constant and the MR arises from the spin-dependent tunneling resistance between the electrodes and the quantum dots. In this model the

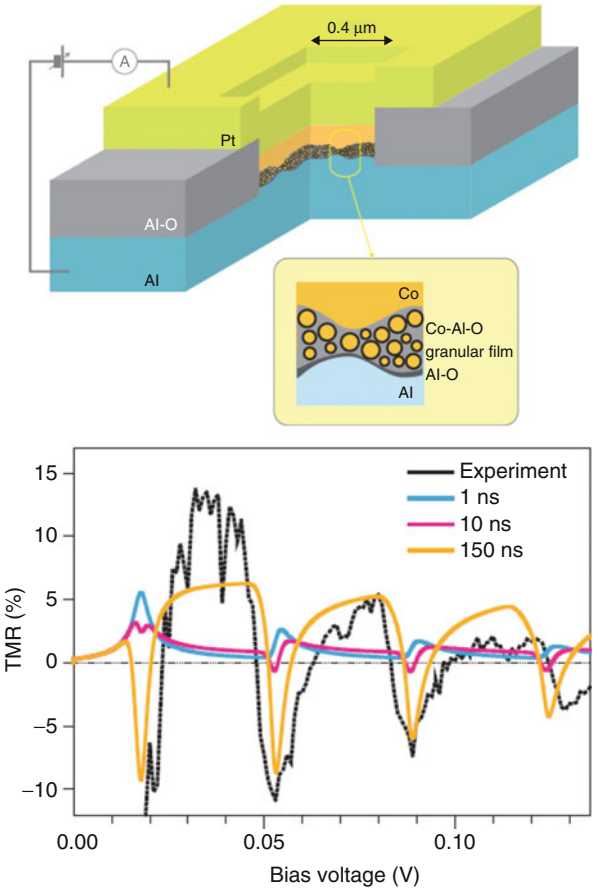

Fig. 24 Yakushiji schematic illustration of Al/Al–O/CoAlO granular tunnel structure; V dependence of the TMR. The *blue*, *pink,* and *orange curves* show the calculated TMR for $\tau SF = 1$ ns, 10 ns, and 150 ns, respectively. The *dotted curve* shows the experimentally observed TMR. The calculated curve assuming the spin-relaxation time of 150 ns reproduces well the experimental one (Reprinted by permission from Macmillan Publishers Ltd: Nature Materials [131], copyright 2005)

Coulomb blockade voltage itself is spin dependent which leads to a much larger MR. This CBMR effect can be realized in organic granular, MTJ, giant magneto-resistance, and colossal magneto-resistance structures. As shown in Fig. 25b, Feng et al. [132] observed over 10,000 % MR ratio in phase-separated $La_{0.67}Sr_{0.33}MnO_3$/$SrTiO_3$/$La_{0.67}S_{r0.33}MnO_3$ MTJs. Quantitative agreement between the model and the experiment for the bias voltage dependence was also observed. This CBMR effect may be promising in designing high signal-to-noise ratio and low power consumption spintronic devices in future.

Spin Transfer Torque Effect in MTJ

Spin-transfer torque (STT) effect is a milestone discovery in the development of spintronics. STT will not only provide a new data writing strategy, but is also consistent with the development trend of high density devices. To reduce the critical switching current is the pursuing target both in lab and industry.

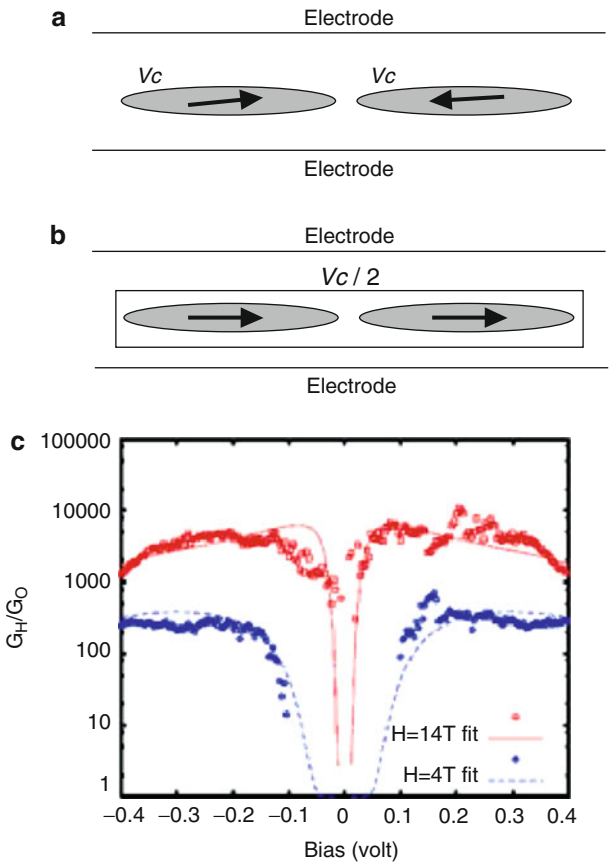

Fig. 25 (**a**) When the moments of two magnetic QDs are antiferromangetically oriented, the CB voltage is *Vc*. (**b**) An external magnetic field aligns the moments of the two dots, the CB voltage is reduced to *Vc* (Reprinted with permission from [12]. Copyright (2010) by the American Physical Society). (**c**) Comparison of the model (*solid* and *dash lines*) with experiment (*square* and *circle*) under different magnetic field in $La_{0.67}Sr_{0.33}MnO_3/SrTiO_3/La_{0.67}S_{r0.33}MnO_3$ MTJ (Reprinted with permission from [132]. Copyright (2008), AIP Publishing LLC)

In 2003, Liu et al. [133] observed current induced magnetic switching with the current as high as tens of micro-Ampere in micro-magnetic tunnel junctions. But this switching process cannot be explained only by the STT effect. The Oester field is also important in this switching process. In 2004, Huai et al. [13] observed obvious STT effect in Al–O MTJs, as shown in Fig. 26a, c are the *R-H* curves (b) and (d) is the current induced switching curve for Al–O MTJs (left), the critical switching current is 8×10^6 A/cm^2.

Han et al. [41, 134] fabricated nano-ring magnetic tunnel junctions (NR-MTJ) with 2.5 nm CoFeB free layer, 100 nm outer diameter, and 25 nm width. The MTJ stack structure consists of Ta(5 nm)/Ru(10)/Ta(5)/$Ni_{81}Fe_{19}$(5)/$Ir_{22}Mn_{78}$(12)/CoFe(2)/Ru(0.9)/CoFeB(3)/Al(0.6-oxide)/CoFeB(2.5)/Ta(5)/Ru(6). The spin-polarized current

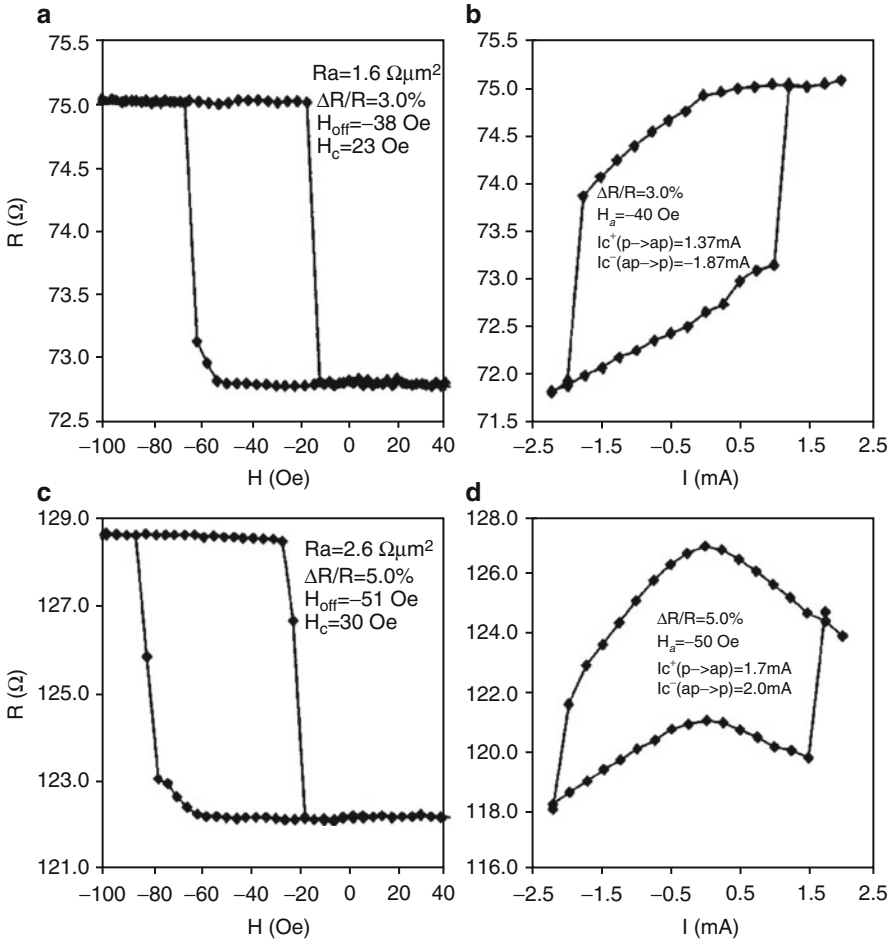

Fig. 26 Field and current induced magnetic switching in Al–O magnetic tunnel junctions (Reprinted with permission from [13]. Copyright (2004), AIP Publishing LLC)

induced magnetic switching was investigated. Figure 27 shows the typical switching curve of NR-MTJ. Pulse current width of 500 ns was exerted on the NR-MTJ. After the introduction of pulse current, 10 μA current was used to measure the resistance. The STT produced by pulse current interact with the magnetic moment of free layer. When the current density reaches the critical value, the free layer is switched. The critical current for AP to P state is 425 μA and P to AP is 475 μA in this NR-MTJ.

Wei et al. [135] studied the current induced magnetic switching in sandwich nano-ring magnetic tunnel junctions. Before each measurement, a 500 ns current pulse was applied to the junctions and then 10 μA current was used to read the resistance. This small measurement current did not affect the domain structure. Repeating the process by increasing or decreasing the amplitude of current, the

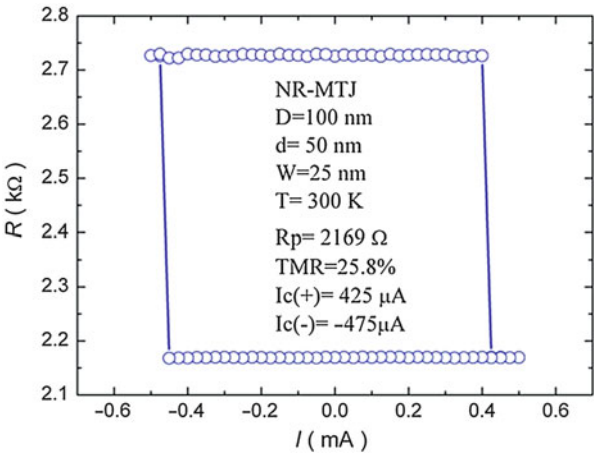

Fig. 27 Spin-polarized current induced switching of nano-ring shaped magnetic tunnel junctions (Reprinted with permission from [134]. Copyright (2007), AIP Publishing LLC)

R-I curve can be obtained as shown in Fig. 28. The critical current for switching from AP to P state is 1.1 mA and the corresponding current density is 6×10^6 A/cm^2.

Wei et al. pointed out that the simulation shows a gradual change in resistance just before switching near the parallel (antiparallel) resistance at positive (negative) currents, while the experimental switching between parallel and antiparallel resistances is abrupt. This discrepancy is due to an artifact in which the simulation was carried out with a constant current density. When the current is near the switching current, one of the layers is in a stable precessional state. Experimentally, the resistance was measured after the pulsed current was switched off. Therefore, the measured states returned to the parallel onion states. The current was turned off after a certain time during the simulation, and the loop did not change gradually because the precessional states returned to either the parallel or antiparallel state (Fig. 28e).

When the current is applied perpendicular to the junctions, besides STT, the current will exert a circular Oersted field. This field will result in complex multiple switching in nano-ring shaped MTJs [136]. Wei et al. [137] studied the multiple switching of NR-MTJ with 100 nm diameter under the combined action of spin-polarized current and the Oersted field. They found that the switching process depends mainly on the non-adiabatic STT, while the circular Oersted field plays a supplementary role.

The Applications of Al–O Based MTJ

Applications of MTJs include hard drive read heads, magnetic random access memories, spin field effect transistors, magnetic logic devices, magnetic sensors, etc. Before 2004, investigations on MTJs and their applications mainly focused on Al–O based MTJs. Studies on physics and applications of Al–O based MTJs not

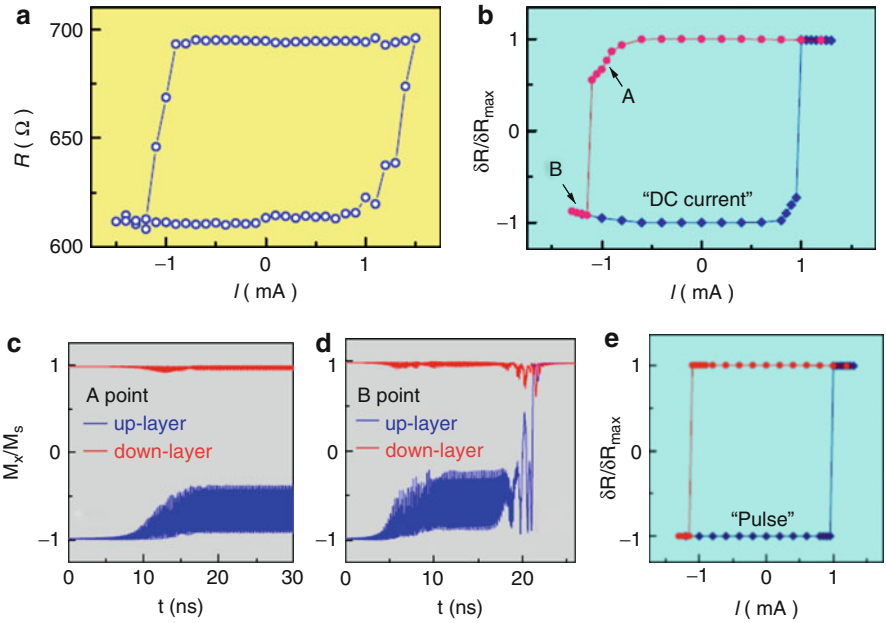

Fig. 28 Current induced magnetic switch in sandwich nano-ring MTJ without magnetic field (Reprinted with permission from [135]. Copyright (2008) by the American Physical Society). The tunnel resistance as a function of the amplitude of the 200 ns pulsed current density at zero magnetic field. (**a**) Experimental results at room temperature. Simulation results of the R-I loop. (**b**) The precessional states near the critical current density. (**c**) The switched state for the current exceeding the critical value. (**d**) The damping parameters of 0.01 and 0.015 for the top and bottom magnetic rings are used for the simulation. (**e**) The simulated R-I curve after the pulsed current is turned off

only paved the way for magnetic electronics and spintronics, but also enormously improved applications of MR materials and novel spintronic devices in information industries. At the same time, investigations on Al–O MTJs laid the foundation for MgO-based MTJs with even higher MR ratio and their applications.

Magnetic Read Heads

Read head, as an important component of hard disk drive, flies on the surface of disk and converts the magnetic field in disk into electric signal. INESC reported in 2000 their first Al–O based MTJ read head which can be used to read information recorded in a hard disk with an areal density of 100 Gbit/in^2 [138]. In the same year, Seagate Technology demonstrated their Al–O based read head [139]. MTJs can be used as read head in hard disk drives if their resistance-area product is smaller than 10 Ωμm^2 and magnetoresistance ratio is greater than 10 % ~ 20 %. Kobayashi et al. [140] summarized developments of Al–O MTJs from 1995 to 2005 (as shown in Fig. 29). Lower MR ratio of Al–O MTJs compared to that of MgO-based ones

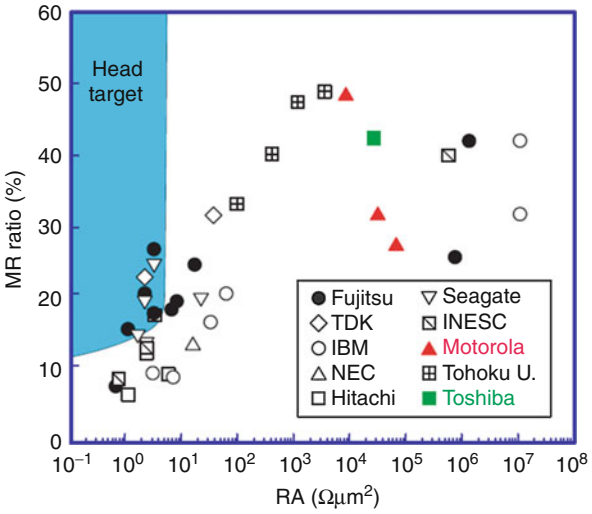

Fig. 29 Relationship between MR ratios and resistance-area product RA in MTJs. [140]

limit their usage in commercial ultrahigh areal density read heads. The first commercial MTJ read head product released by Seagate Technology in 2005 was based on MgO [141].

Magnetic Sensors

Al–O based MTJs can be used in various commercial magnetic sensors. Compared to widely used semiconductor-based Hall devices, magnetic sensors based on MTJs have irreplaceable advantages. MTJ based sensors also show higher sensitivity. Ordinary commercial spin valve GMR sensors show an MR ratio of about 10 % at room temperature and the sensitivity is usually not higher than 10 mV/Oe, even when inserted into a bridge circuit. However, Al–O based spin valve shows MR ratio of 50–80 % and hence higher sensitivity in detection of tiny magnetic fields [142, 143], because of which MTJs are competitive in the field of magnetic sensor. Particularly, the most important advantage of MTJs is that their sizes can be patterned down to micrometers and even hundreds of nanometers. As a result, MTJ sensors have high spatial resolution and can be used as biological sensors [144–146].

Magnetic Random Access Memory (MRAM)

Another important application of TMR effect is to use the change of resistance for non-violate information storage. Resistance difference of MTJs in their two most stable magnetic configurations, i.e., parallel and antiparallel configurations, can be used to store the two independent states in electronic information as 0 and 1.

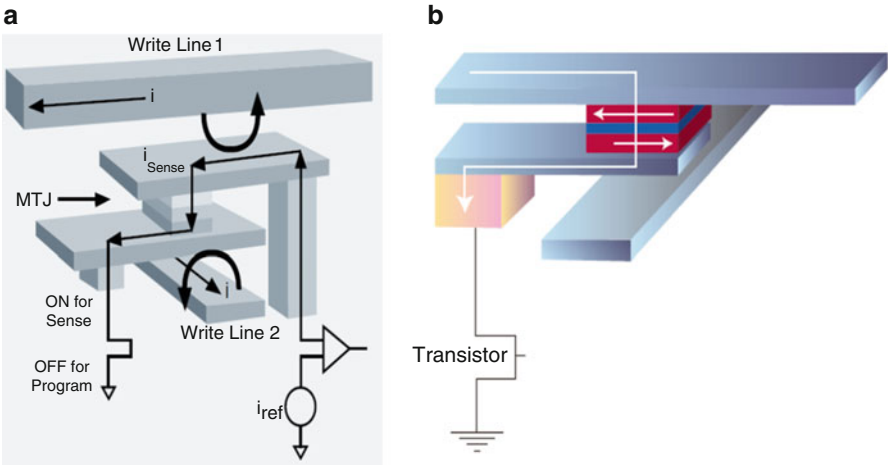

Fig. 30 Schematic graph of (**a**) field driven MRAM cell constructed from "1T + 1MTJ" structure and (**b**) electric current driven spin transfer torque MRAM cell

As a result, MTJ based on TMR effect can be used to develop novel random access memories, i.e., magnetic random access memory (MRAM). MRAM takes the advantages of low energy consumption, non-volatility, and can package information accessing, transferring, processing, and storage into one chip (Fig. 30).

In the history of MRAM, Al–O based MTJ played a crucial role. MRAM has attained a great progress thanks to researchers' contributions. MRAM has developed from astroid MRAM, toggle MRAM, and thermal assisted MRAM which are read and written by magnetic field, to spin-transfer MRAM and nano-ring MRAM which are read and written by spin-polarized electric current [41]. Investigations in recent years showed that MRAM based on spin-transfer torque has the potential to develop MRAM with higher areal density and, hence, higher capacity, which is the goal of companies all over the world. Up to now, the development of MRAM can be illustrated by Fig. 31 [41].

In summary, along with continuous effort in investigations of spin-transfer MRAM, it is not hard to predict that in the near future, spin-transfer MRAM with high performance and high capacity would appear in commercial applications. The progress of MRAM is covered in Part IX, Volume 2.

Spin Transistors and Field Effect Transistors

Spin transistor with memory and logic functions is one of the potential applications of MR effect and its usage in future powerful integrated circuits has gained much attention. Typical structures of spin transistor [147, 148] is shown in Fig. 32. Voltage applied across MTJ is usually smaller than 0.5 V and the spin-dependent scattering occurs near Fermi level. In contrast, collector electrode in spin transistor

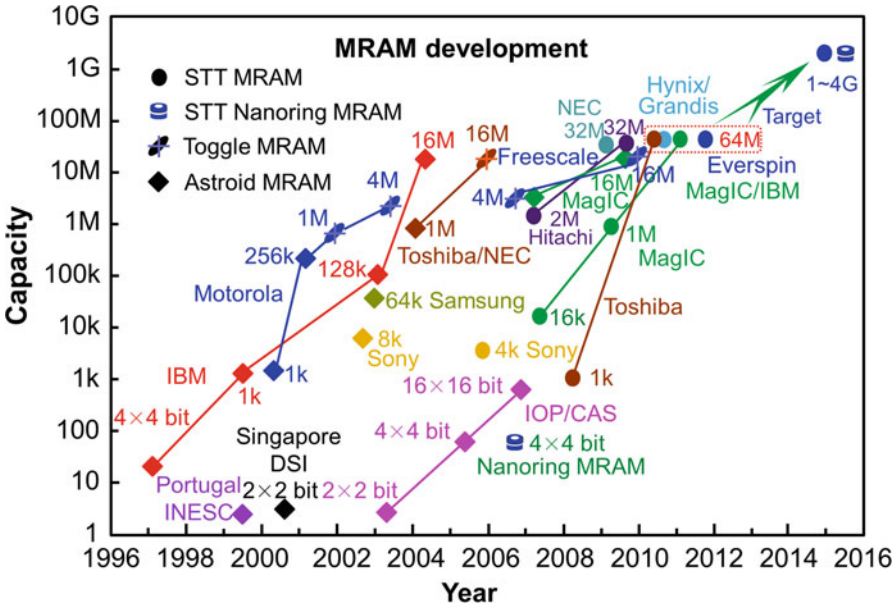

Fig. 31 Roadmap of MRAM demo device development for both the conventional Astroid or Toggle design using magnetic-field-driving method and the novel STT-MRAM or nanoring MRAM design using current-switching method based on one MTJ and one transistor structure (Reprinted with permission from [41]. Copyright (2008), AIP Publishing LLC)

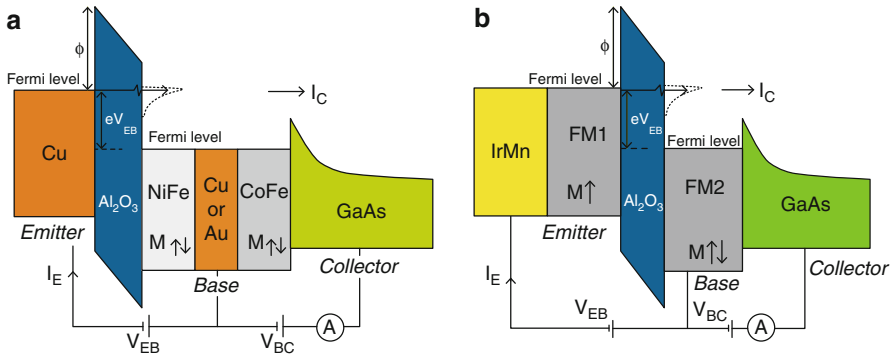

Fig. 32 (**a**) Schematic energy diagram of the MTT device showing a Cu emitter separated from the spin-valve base layer by an Al_2O_3 tunneling barrier. The spin valve is comprised of ferromagnetic CoFe and NiFe layers separated by Au or Cu spacer layers. The energy of the injected hot electrons is varied by varying the emitter/base bias voltage. The Schottky barrier formed at the interface between the spin-valve base layer and the GaAs collector is slightly reverse-biased in these experiments (Reprinted with permission from [148]. Copyright (2003), AIP Publishing LLC). (**b**) Schematic energy diagram for an MTJ with a single FM base layer (© (2003) IEEE. Reprinted with permission from [149])

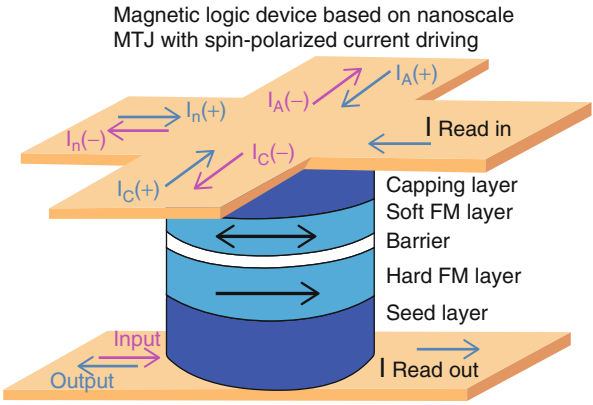

Fig. 33 Schematic graph of magnetic logic device based on nano-scale MTJ with spin-polarized current driving [152]

collects hot electrons and energy differences between these hot electrons and Fermi level is usually several volts. Electrons injected from emitter electrode are strongly scattered spin-dependently in base electrode and finally these highly spin-polarized electrons tunnel from collector electrode to semiconductor which is connected with collector electrode. Therefore, spin polarized electrons injection into semiconductor can be realized [149].

Magnetic Logic Devices

Digital logic design using spin of electrons in magnetic materials is magnetic logic. MTJs based on TMR effect have been widely used in data storage and magnetic field sensor; however, their application in magnetic logic is still at beginning stage. Das proposed a kind of spin magnetic logic [150] based on MR effect driven by magnetic field in 2000. Two years later, Siemens demonstrated a kind of magnetic logic element which can be renewed. Magnetic logic devices driven by spin-polarized current is easy to fabricate and to control because of simple structure and low power consumption [151, 152] (Fig. 33).

Memristors

In early 1971, Chua [153] firstly proposed the concept of memristor in theory. The concept of memristor was proved in experiments by Stanley Williams Lab in 2008 [154]. Resistance of memristor depends on integral of voltage and current and the history of applied voltage and current can be memorized by memristor. Electric field induced resistance switching in oxides has been widely investigated and the mechanism was attributed to drift of oxygen atoms under bias electric field. MR effect and electric field induced resistance switching can be observed in Al–O based and MgO based MTJs at the same time. However, simultaneous observation of MR effect and electric field induced resistance switching is on its beginning stage. Krzysteczko

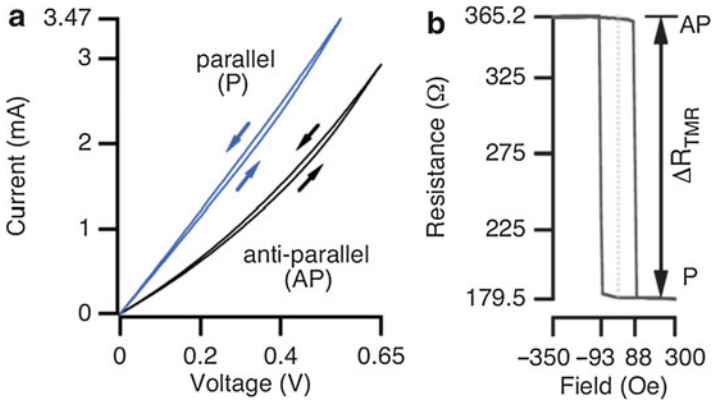

Fig. 34 Simultaneous occurrence of resistive and magnetoresistive switching in CoFeB/MgO/CoFeB MTJ. (**a**) A slight splitting of I-V curve can be observed for both magnetic states, which demonstrates the presence of resistance switching. Since the curves are highly symmetric with respect to the origin, only the first quadrant is shown. (**b**) The magnetoresistive switching of the device characterized by a magnetic minor loop (Reprinted with permission from [155]. Copyright (2009), AIP Publishing LLC)

et al. [155] successfully observed MR effect and electric field induced resistance switching in CoFeB/MgO/CoFeB MTJs. In their work, they observed MR ratio of 100 % and electric field induced resistance change of 6 %. For parallel and antiparallel magnetic configurations, electric field applied on MTJs can induce multi-resistance state, as shown in Fig. 34, which can be used in multi-state data storage.

Summary and Prospects on Al–O MTJs

The discovery and development of Al–O magnetic tunnel junctions is a milestone of great significance in magnetic tunnel junctions and spintronics. In 1995, the large MR ratio at room temperature was reported for the first time in Al–O MTJ [2, 3] after 20 years of remarkable achievements. Based on these achievements, the progress on MgO-MTJs was started in 2001 [156–158]. Although, at present over 100 % TMR ratio can be obtained in Al–O MTJs [51] and over 600 % TMR ratio in single crystalline MgO-MTJs [159] at room temperature, it is still possible to get MTJs with higher TMR and better performance by searching new barrier and magnetic electrode materials. For example, recently, spinel oxides AB_2O_4 [160] have drawn much attention due to their rich electric and magnetic properties and small lattice mismatch (<1 %) with typical ferromagnetic metallic electrode materials such as Fe, Co, CoFeB, and Heusler alloy. In 2010, scientists in NIMS have successfully fabricated Fe/$MgAl_2O_4$/Fe magnetic tunnel junctions. Preliminary results show that the MTJ has good magneto-electric performance. The TMR exceeds 110 % at room temperature, the half-width is as high as 1 V [161]. By carrying out first-principles calculations, Zhang et al. [162] found that several

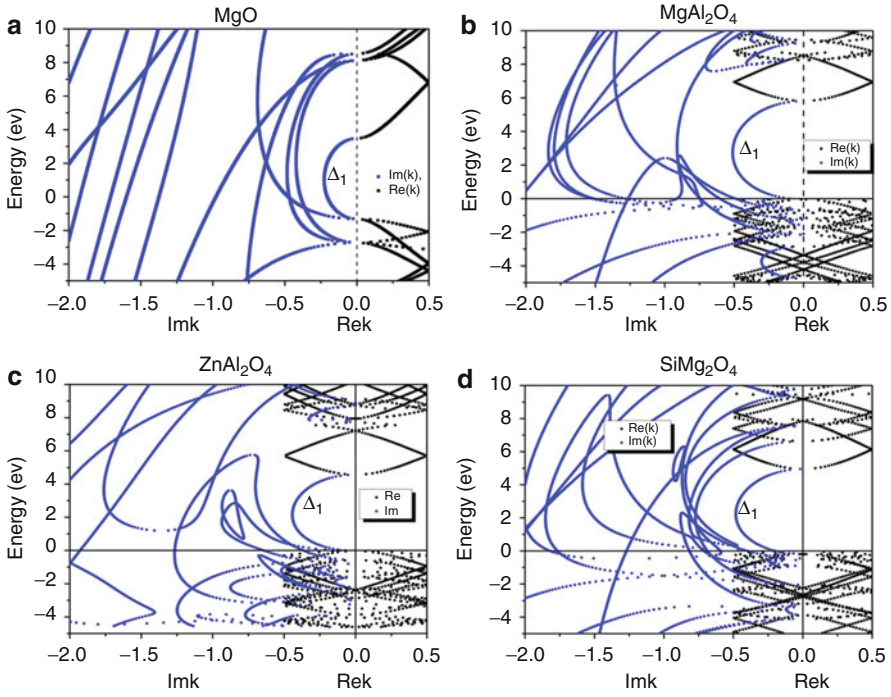

Fig. 35 The band structure of (**a**) MgO, (**b**) spinel $MgAl_2O_4$, (**c**) spinel $ZnAl_2O_4$, and (**d**) spinel $SiMg_2O_4$ long [001] direction. The *blue* and *black curves* show the pure imaginary and real bands, respectively. These spinel oxides have similar Δ_1 spin-filter effect as MgO (Reprinted with permission from [162]. Copyright (2012), AIP Publishing LLC)

typical spinel oxides have the similar complex band like MgO. It is promising to get high TMR in MTJ with this kind of spinel oxides, as shown in Fig. 35. The magnetic electrodes with high spin-polarization, perpendicular magnetic anisotropy [163] and low damping parameter [164] have important application value on the high speed, low power consumption spintronic devices such as magnetic random access memory and nano-oscillator, etc.

In conclusion, the Al–O based MTJ fabrication and its high TMR ratio observed is not only a milestone discovery, its rich material and device applications is also a very important constituent part in developing magneto-electronics and spintronics.

References

1. Julliére M (1975) Tunneling between ferromagnetic films. Phys Lett A 54:225
2. Miyazaki T, Tezuka N (1995) Giant magnetic tunneling effect in Fe/Al_2O_3/Fe junction. J Magn Magn Mater 139:L231
3. Moodera JS, Kinder LR, Wong TM, Meservey R (1995) Large magnetoresistance at room temperature in ferromagnetic thin film tunnel junctions. Phys Rev Lett 74:3273

4. Wei HX, Qin QH, Ma M, Sharif R, Han XF (2007) 80 % TMR at room temperature for thin Al–O barrier magnetic tunnel junction with CoFeB as free and reference layers. J Appl Phys 101:09B501
5. Žutić I, Fabian J, Das Sarma S (2004) Spintronics: fundamentals and applications. Rev Mod Phys 76:323
6. Ohno H, Shen A, Matsukura F, Oiwa A, Endo A, Katsumoto S, Iye Y (1996) (Ga,Mn)As: a new diluted magnetic semiconductor based on GaAs. Appl Phys Lett 69:363
7. Du GX, Babu MR, Han XF, Deng JJ, Wang WZ, Zhao JH, Wang WD, Jinke Tang (2009) Tunneling magnetoresistance in (Ga,Mn)As/Al–O/CoFeB hybrid structures. J Appl Phys 105:07C707
8. Chang Y-M, Li KS, Chiang W-C, Lin M-T (2009) Superconductivity-induced magnetoresistance suppression in hybrid superconductor/magnetic tunnel junctions. Phys Rev B 79:012401
9. Sheng L, Chen Y, Teng HY, Ting CS (1999) Nonlinear transport in tunnel magnetoresistance systems. Phys Rev B 59:480
10. Montaigne F, Nassar J, Vaurès A, Nguyen Van Dau F, Petroff F, Schuhl A, Fert A (1997) Enhanced tunnel magnetoresistance at high bias voltage in double-barrier planar junctions. Appl Phys Lett 73:2829
11. Saito Y, Amano M, Nakajima K, Takahashi S, Sagoi M, Inomata K (2000) Correlation between barrier width, barrier height, and DC bias voltage dependences on the magnetoresistance ratio in Ir–Mn exchange biased single and double tunnel junctions. Jpn J Appl Phys 39:L1035
12. Zhang X-G, Wen ZC, Wei HX, Han XF (2010) Giant Coulomb blockade magnetoresistance in magnetic tunnel junctions with a granular layer. Phys Rev B 81:155122
13. Huai Y, Albert F, Nguyen P, Pakala M, Valet T (2004) Observation of spin-transfer switching in deep submicron-sized and low-resistance magnetic tunnel junctions. Appl Phys Lett 84:3118
14. Slonczewski JC (1989) Conductance and exchange coupling of two ferromagnets separated by a tunneling barrier. Phys Rev B 39:6995
15. Berger L (1984) Exchange interaction between ferromagnetic domain wall and electric current in very thin metallic films. J Appl Phys 55:1954
16. Tehrani S, Slaughter JM, Deherrera M et al (2003) Magnetoresistive random access memory using magnetic tunnel junctions. Proc IEEE 91:703
17. Enge BN, Akerman J, Butcher B et al (2005) A 4-Mb toggle MRAM based on a novel bit and switching method. IEEE Trans Magn 41:132
18. Bader SD, Parkin SSP (2010) Annual review of condensed matter physics. Spintronics 1:71
19. Matsuda K, Kamijo A, Mitsuzuka T, Tsuge H (1999) Exchange-biased magnetic tunnel junctions fabricated with in situ natural oxidation. J Appl Phys 85:5261
20. Parkin SSP, Roche KP, Samant MG, Rice PM, Beyers RB, Scheuerlein RE, O'Sullivan EJ, Brown SL, Bucchigano J, Abraham DW, Yu Lu, Rooks M, Trouilloud PL, Wanner RA, Gallagher WJ (1999) Exchange-biased magnetic tunnel junctions and application to nonvolatile magnetic random access memory (invited). J Appl Phys 85:5828
21. Zhang ZG, Freitas PP, Ramos AR, Barradas NP, Soares JC (2001) Resistance decrease in spin tunnel junctions by control of natural oxidation conditions. Appl Phys Lett 79:2219
22. Boeve H, De Boeck J, Borghs G (2001) Low-resistance magnetic tunnel junctions by in situ natural oxidation. J Appl Phys 89:482
23. Gallagher WJ, Parkin SSP, Yu Lu, Bian XP, Marley A, Roche KP, Altman RA, Rishton SA, Jahnes C, Shaw TM, Gang Xiao (1997) Microstructured magnetic tunnel junctions (invited). J Appl Phys 81:3741
24. Han XF, Oogane M, Kubota H, Ando Y, Miyazaki T (2000) Fabrication of high-magnetoresistance tunnel junctions using $Co_{75}Fe_{25}$ ferromagnetic electrodes. Appl Phys Lett 77:283

25. Sousa RC, Sun JJ, Soares V, Freitas PP, Kling A, da Silva MF, Soares JC (1998) Large tunneling magnetoresistance enhancement by thermal anneal. Appl Phys Lett 73:3288
26. LeClair P, Kohlhepp JT, Smits AA, Swagten HJM, Koopmans B, de Jonge WJM (2000) Optical and in situ characterization of plasma oxidized Al for magnetic tunnel junctions. J Appl Phys 87:6070
27. Wang D, Nordman C, Daughton JM, Qian Z, Fink J (2004) 70 % TMR at room temperature for SDT sandwich junctions with CoFeB as free and reference layers. IEEE Trans Magn 40:2269
28. Shimazawa K, Kasahara N, Sun JJ, Araki S, Morita H, Matsuzaki M (2000) Electrical breakdown of the magnetic tunneling junction with an AlO_x barrier formed by radical oxidation. J Appl Phys 87:5194
29. Boevea H, Girgis E, Schelten J, De Boeck J, Borghs G (2000) Strongly reduced bias dependence in spin–tunnel junctions obtained by ultraviolet light assisted oxidation. Appl Phys Lett 76:1048
30. Rottländer P, Kohlstedt H, Grünberg P, Girgis E (2000) Ultraviolet light assisted oxidation for magnetic tunnel junctions. J Appl Phys 87:6067
31. May U, Samm K, Kittur H, Hauch J, Calarco R, Rüdigera U, Güntherodt G (2001) Temperature-dependent magnetoresistance of magnetic tunnel junctions with ultraviolet light-assisted oxidized barriers. Appl Phys Lett 78:2026
32. Zhu T, Xiang X, Shen F, Zhang Z, Landry G, Dimitrov DV, García N, Xiao JQ (2002) Bulk contributions to tunnel magnetoresistance in magnetic tunnel junctions. Phys Rev B 66:094423
33. Shen F, Zhu T, Xiang XH, Xiao JQ, Voelkl E, Zhang Z (2003) Observation of the barrier structure in magnetic tunnel junctions using high-resolution electron microscopy and electron holography. Appl Phys Lett 83:5482
34. Sato M, Kobayshi K (1997) Spin-valve-like properties and annealing effect in ferromagnetic tunnel junctions. IEEE Trans Magn 33:3553
35. Sato M, Kikuchi H, Kobayashi K (1998) Ferromagnetic tunnel junctions with plasma-oxidized Al barriers and their annealing effects. J Appl Phys 83:6691
36. Tehrani S, Slaughter JM, Chen E, Durlam M, Shi J, DeHerrera M (1999) Progress and outlook for MRAM technology. IEEE Trans Magn 35:2814
37. Sun JJ, Shimazawa K, Kasahara N, Sato K, Saruki S, Kagami T, Redon O, Araki S, Morita H, Matsuzaki M (2000) Low resistance and high thermal stability of spin-dependent tunnel junctions with synthetic antiferromagnetic CoFe/Ru/CoFe pinned layers. Appl Phys Lett 76:2424
38. Cardoso S, Freitas PP, de Jesus C, Wei P, Soares JC (2000) Spin-tunnel-junction thermal stability and interface interdiffusion above 300 °C. Appl Phys Lett 76:610
39. Jun Soo Bae, Kyung Ho Shin, Taek Dong Lee, Hyuck Mo Lee (2002) Study of the effect of natural oxidation and thermal annealing on microstructures of AlOx in the magnetic tunnel junction by high-resolution transmission electron microscopy. Appl Phys Lett 80:1168
40. Wang Y, Zeng ZM, Han XF, Zhang XG, Sun XC, Zhang Z (2007) Temperature-dependent Mn-diffusion modes in CoFeB- and CoFe-based magnetic tunnel junctions: electron-microscopy studies. Phys Rev B 75:214424
41. Han XF, Wen ZC, Wei HX (2008) Nanoring magnetic tunnel junction and its application in magnetic random access memory demo devices with spin-polarized current switching. J Appl Phys 103:07E933
42. Ikeda S, Hayakawa J, Ashizawa Y, Lee YM, Miura K, Hasegawa H, Tsunoda M, Matsukura F, Ohno H (2008) Tunnel magnetoresistance of 604 % at 300 K by suppression of Ta diffusion in CoFeB/MgO/CoFeB pseudo-spin-valves annealed at high temperature. Appl Phys Lett 93:082508
43. Dieny B, Speriosu VS, Parkin SSP, Gurney BA, Wilhoit DR, Mauri D (1991) Giant magnetoresistive in soft ferromagnetic multilayers. Phys Rev B 43:1297

44. Zeng ZM, Jiang LX, Du GX, Zhan WS, Han XF (2006) Hightunnel magnetoresistance in Co–Fe–B based double barrier magnetic tunnel junction. J Magn Mater Magn 303:e219
45. Lee H, Chang IW, Byun SJ, Hong TK, Rhie K, Lee WY, Shin KH, Hwang CY, Lee SS, Lee BC (2002) TMR of double spin-valve type AF/FM/I/FM/I/FM/AF magnetic tunneling junctions. J Magn Magn Mater 240:137
46. Han XF, Zhao SF, Li FF, Daibou T, Kubota H, Ando Y, Miyazaki T (2004) Switching properties and dynamic domain structures in double barrier magnetic tunnel junctions. J Magn Magn Mater 282:225
47. Zhao SF, Zhao J, Zeng ZM, Han XF, Ando Y, Miyazaki T (2005) Tunneling current-induced butterfly-shaped domains and magnetization switching in double-barrier magnetic tunnel junctions. IEEE Trans Magn 41:2636
48. Colis S, Gieres G, Bar L, Wecker J (2003) Low tunnel magnetoresistance dependence versus bias voltage in double barrier magnetic tunnel junction. Appl Phys Lett 83:948
49. Tanaka CT, Nowak J, Moodera JS (1997) Magnetoresistance in ferromagnet-insulator-ferromagnet tunnel junctions with half-metallic ferromagnet NiMnSb compound. J Appl Phys 81:5515
50. Inomata K, Okamura S, Goto R, Tezuka N (2003) Large tunneling magnetoresistance at room temperature using a Heusler alloy with the B2 structure. Jpn J Appl Phys 42:L419
51. Sakuraba Y, Nakata J, Oogane M, Kubota H, Ando Y, Sakuma A, Miyazaki T (2005) Huge spin-polarization of L2(1)-ordered CO_2 MnSi epitaxial Heusler alloy film. Jpn J Appl Phys Part 2 44:L1100
52. Wei HX, Qin QH, Wen ZC, Han XF, Zhang X-G (2009) Magnetic tunnel junction sensor with Co/Pt perpendicular anisotropy ferromagnetic layer. Appl Phys Lett 94:172902
53. Nishimura N, Hirai T, Koganei A, Ikeda T, Okano K, Skiguchi Y, Osada Y (2002) Magnetic tunnel junction device with perpendicular magnetization films for high-density magnetic random access memory. J Appl Phys 91:5246
54. Dongwon Lim, Sungdong Kim, Seong-Rae Lee (2005) Magnetoresistance behavior of a magnetic tunnel junction with perpendicularly magnetized Co/Pd multilayers. J Appl Phys 97:10C902
55. Yu GQ, Chen L, Rizwan S, Zhao JH, XU K, Han XF (2011) Improved tunneling magneto-resistance in (Ga,Mn)As/AlOx/CoFeB magnetic tunnel junctions. Appl Phys Lett 98:262501
56. Jiang JS, Davidović D, Reich DH, Chien CL (1995) Oscillatory superconducting transition-temperature in Nb/Gd multilayers. Phys Rev Lett 74:314
57. Moraru IC, Pratt WP Jr, Birge NO (2006) Magnetization-dependent T-c shift in ferromagnet/superconductor/ferromagnet trilayers with a strong ferromagnet. Phys Rev Lett 96:037004
58. Giroud M, Courtois H, Hasselbach K, Mailly D, Pannetier B (1998) Superconducting proximity effect in a mesoscopic ferromagnetic wire. Phys Rev B 58:11872
59. Petrashov VT, Sosnin IA, Cox I, Parsons A, Troadec C (1999) Giant mutual proximity effects in ferromagnetic/superconducting nanostructures. Phys Rev Lett 83:3281
60. Dubonos SV, Geim AK, Novoselov KS, Grigorieva IV (2002) Spontaneous magnetization changes and nonlocal effects in mesoscopic ferromagnet-superconductor structures. Phys Rev B 65:220513(R)
61. Hong-ye Wu, Jing Ni, Jian-wang Cai, Zhao-hua Cheng, Young Sun (2007) Experimental evidence of magnetization modification by superconductivity in a Nb/Ni81Fe19 multilayer. Phys Rev B 76:024416
62. Monton C, de la Cruz F, Guimpel J (2008) Magnetic state modification induced by superconducting response in ferromagnet/superconductor Nb/Co superlattices. Phys Rev B 77:104521
63. Gittleman JI, Goldstein Y, Bozowski S (1972) Magnetic properties of granular nickel films. Phys Rev B 5:3609
64. Helman JS, Abeles B (1976) Tunneling of spin-polarized electrons and magnetoresistance in granular Ni films. Phys Rev Lett 37:1429

65. Fujimori H, Mitania S, Ohnumab S (1995) Tunnel-type GMR in metal-nonmetal granular alloy thin films. Mater Sci Eng B 31:219
66. Luryi S (1985) Frequency limit of double-barrier resonant-tunneling oscillators. Appl Phys Lett 47:490
67. Averin DV, Nazarov YV (1990) Virtual electron diffusion during quantum tunneling of the electric charge. Phys Rev Lett 65:2446
68. Takahashi S, Maekawa S (1998) Effect of Coulomb blockade on magnetoresistance in ferromagnetic tunnel junctions. Phys Rev Lett 80:1758
69. Mitania S, Fujimoria H, Ohnumab S (1997) Spin-dependent tunneling phenomena in insulating granular systems. J Magn Magn Mater 165:141
70. Shang CH, Nowak J, Jansen R, Moodera JS (1998) Temperature dependence of magnetoresistance and surface magnetization in ferromagnetic tunnel junctions. Phys Rev B 58:R2917
71. Moodera JS, Nowak J, van de Veerdonk RJM (1998) Interface magnetism and spin wave scattering in ferromagnet-insulator-ferromagnet tunnel junctions. Phys Rev Lett 80:2941
72. MacDonald AH, Jungwirth T, Kasner M (1998) Temperature dependence of itinerant electron junction magnetoresistance. Phys Rev Lett 81:705
73. Garcia V, Bibes M, Barthélémy A, Bowen M, Jacquet E, Contour J-P, Fert A (2004) Temperature dependence of the interfacial spin polarization of $La_{2/3}Sr_{1/3}MnO_3$. Phys Rev B 69:052403
74. Wang SG, Ward RCC, Du GX, Han XF, Wang C, Kohn A (2008) Temperature dependence of giant tunnel magnetoresistance in epitaxial Fe/MgO/Fe magnetic tunnel junctions. Phys Rev B 78:180411(R)
75. Shan R, Sukegawa H, Wang WH, Kodzuka M, Furubayashi T, Ohkubo T, Mitani S, Inomata K, Hono K (2009) Demonstration of half-metallicity in fermi-level-tuned Heusler alloy $Co_2FeAl_{0.5}Si_{0.5}$ at room temperature. Phys Rev Lett 102:246601
76. Zhang S, Levy PM, Marley AC, Parkin SSP (1997) Quenching of magnetoresistance by hot electrons in magnetic tunnel junctions. Phys Rev Lett 79:3744
77. Bratkovsky AM (1997) Tunneling of electrons in conventional and half-metallic systems: towards very large magnetoresistance. Phys Rev B 56:2344
78. Bratkovsky AM (1998) Assisted tunneling in ferromagnetic junctions and half-metallic oxides. Appl Phys Lett 72:2334
79. Vedyayev A, Bagrets D, Bagrets A, Dieny B (2001) Resonant spin-dependent tunneling in spin-valve junctions in the presence of paramagnetic impurities. Phys Rev B 63:064429
80. Yuasa S, Sato T, Tamura E, Suzuki Y, Yamamori H, Ando K, Katayama T (2000) Magnetic tunnel junctions with single-crystal electrodes: a crystal anisotropy of tunnel magnetoresistance. Europhys Lett 52:344
81. Boeve H, Girgis E, Schelten J, De Boeck J, Borghs G (2000) Strongly reduced bias dependence in spin–tunnel junctions obtained by ultraviolet light assisted oxidation. Appl Phys Lett 76:1048
82. Ahn SJ, Kato T, Kubota H, Ando Y, Miyazaki T (2005) Bias-voltage dependence of magnetoresistance in magnetic tunnel junctions grown on Al_2O_3 (0001) substrates. Appl Phys Lett 86:102506
83. Ma QL (2011) Optimization and magneto-electronic transport properties of MgO based magnetic tunnel junctions. PhD thesis
84. Han XF, Andrew CC, Yu, Oogane M, Murai J, Daibou T, Miyazaki T (2001) Analyses of intrinsic magnetoelectric properties in spin-valve-type tunnel junctions with high magnetoresistance and low resistance. Phys Rev B 63:224404
85. Lu C, Wu MW, Han XF (2003) Magnon- and phonon-assisted tunneling in a high-magnetoresistance tunnel junction using Co75Fe25 ferromagnetic electrodes. Phys Lett A 319:205
86. Jansen R, Moodera JS (1998) Influence of barrier impurities on the magnetoresistance in ferromagnetic tunnel junctions. J Appl Phys 83:6682

87. Jansen R, Moodera JS (2000) Magnetoresistance in doped magnetic tunnel junctions: effect of spin scattering and impurity-assisted transport. Phys Rev B 61:9047
88. Ding HF, Wulfhekel W, Henk J, Bruno P, Kirschner J (2003) Absence of zero-bias anomaly in spin-polarized vacuum tunneling in Co(0001). Phys Rev Lett 90:116603
89. Zhang J, White RM (1998) Voltage dependence of magnetoresistance in spin dependent tunneling junctions. J Appl Phys 83:6512
90. Davis H, Maclaren JM (2000) Spin dependent tunneling at finite bias. J Appl Phys 87:5224
91. Cabrera G, García N (2002) Low voltage I–V characteristics in magnetic tunneling junctions. Appl Phys Lett 80:1782
92. Sharma M, Wang SX, Nickel JH (1999) Inversion of spin polarization and tunneling magnetoresistance in spin-dependent tunneling junctions. Phys Rev Lett 82:616
93. LeClair P, Kohlhepp JT, van de Vin CH, Wieldraaijer H, Swagten HJM, de Jong WJM (2002) Band structure and density of states effects in co-based magnetic tunnel junctions. Phys Rev Lett 88:107201
94. Sadamichi M, Teruya S (2002) Spin dependent transport in magnetic nanostructures, Chap 3. Taylor & Francis, London, p 132
95. Ando Y, Murai J, Kubota H, Miyazaki T (2000) Magnon-assisted inelastic excitation spectra of a ferromagnetic tunnel junction. J Appl Phys 87:5209
96. Appelbaum J (1966) "s-d" exchange model of zero-bias tunneling anomalies. Phys Rev Lett 17:91
97. Anderson PW (1966) Localized magnetic states and fermi-surface anomalies in tunneling. Phys Rev Lett 17:95
98. Joel A (1967) Appelbaum, exchange model of zero-bias tunneling anomalies. Phys Rev 154:633
99. Wei HX, Qin QH, Ma QL, Zhang XG, Han XF (2010) Signatures of surface magnon and impurity scatterings in tunnel junctions. Phys Rev B 82:134436
100. Zhang X, Li B-Z, Sun G, Fu-Cho P (1997) Spin-polarized tunneling and magnetoresistance in ferromagnet/insulator (semiconductor) single and double tunnel junctions subjected to an electric field. Phys Rev B 56:5484
101. Vedyayev A, Ryzhanova N, Lacroix C, Giacomoni L, Dieny B (1997) Resonance in tunneling through magnetic valve tunnel junctions. Europhys Lett 39:219
102. Mathon J, Umerski A (1999) Theory of tunneling magnetoresistance in a junction with a nonmagnetic metallic interlayer. Phys Rev B 60:1117
103. Moodera JS, Nowak J, Kinder LR, Tedrow PM, van de Veerdonk RJM, Smits BA, van Kampen M, Swagten HJM, de Jonge WJM (1999) Quantum well states in spin-dependent tunnel structures. Phys Rev Lett 83:3029
104. LeClair P, Swagten HJM, Kohlhepp JT, van de Veedonk RJM, de Jonge WJM (2000) Apparent spin polarization decay in Cu-dusted Co/Al_2O_3/Co tunnel junctions. Phys Rev Lett 84:2933
105. LeClair P, Kohlhepp JT, Swagten HJM, de Jonge WJM (2001) Interfacial density of states in magnetic tunnel junctions. Phys Rev Lett 86:1066
106. Yuasa S, Nagahama T, Suzuki Y (2002) Spin-polarized resonant tunneling in magnetic tunnel junctions. Science 297:234
107. Matsumoto R, Fukushima A, Yakushiji K, Nishioka S, Nagahama T, Katayama T, Suzuki Y, Ando K, Yuasa S (2009) Spin-dependent tunneling in epitaxial Fe/Cr/MgO/Fe magnetic tunnel junctions with an ultrathin Cr(001) spacer layer. Phys Rev B 79:174436
108. Greullet F, Tiusan C, Montaigne F, Hehn M, Halley D, Bengone O, Bowen M, Weber W (2007) Evidence of a symmetry-dependent metallic barrier in fully epitaxial MgO based magnetic tunnel junctions. Phys Rev Lett 99:187202
109. Wang Y, Zhang J, Zhang X-G, Cheng H-P, Han XF (2010) First-principles study of Fe/MgO based magnetic tunnel junctions with Mg interlayers. Phys Rev B 82:054405
110. Zhang J, Wang Y, Zhang X-G, Han XF (2010) Inverse and oscillatory magnetoresistance in Fe(001)/MgO/Cr/Fe magnetic tunnel junctions. Phys Rev B 82:134449

111. Zhang XD, Li B-Z, Sun G, Pu F-C (1998) Spin-polarized resonant tunneling and quantum-size effect in ferromagnetic tunnel junctions with double barriers subjected to an electric field. Phys Lett A 245:133
112. Zhang X, Li B, Sun G, Fucho P (1998) Giant tunneling magnetoresistance in ferromagnet/insulator (semiconductor) coupling double-tunnel junction subjected to electric field. Sci China Ser A Math 41:177
113. Barnas J, Fert A (1998) Magnetoresistance oscillations due to charging effects in double ferromagnetic tunnel junctions. Phys Rev Lett 80:1058
114. Barnas J, Fert A (1999) Interplay of spin accumulation and Coulomb blockade in double ferromagnetic junctions. J Magn Magn Mater 192:L391
115. Vedyayev A, Ryzhanova N, Vlutters R, Dieny B, Strelkov N (2000) Giant tunnel magnetoresistance in multilayered metal/oxide structures comprising multiple quantum wells. J Phys Condens Matter 10:5799
116. Vedyayev A, Ryzhanova N, Vlutters A, Dieny B, Strelkov N (2000) Voltage dependence of giant tunnel magnetoresistance in triple barrier magnetic systems. J Phys Condens Matter 12:1797
117. Zeng ZM, Han XF, Zhan WS, Wang Y, Zhang Z, Zhang S (2005) Oscillatory tunnel magnetoresistance in double barrier magnetic tunnel junctions. Phys Rev B 72:054419
118. Valet T, Fert A (1993) Theory of the perpendicular magnetoresistance in magnetic multilayers. Phys Rev B 48:7099
119. Berger L (1996) Emission of spin waves by a magnetic multilayer traversed by a current. Phys Rev B 54:9353
120. Zheng Z, Qi Y, Xing DY, Dong J (1999) Oscillating tunneling magnetoresistance in magnetic double-tunnel-junction structures. Phys Rev B 59:14505
121. Wilczynski M, Barnas J (2000) Tunnel magnetoresistance in ferromagnetic double-barrier planar junctions: coherent tunneling regime. J Magn Magn Mater 221:373
122. Wilczynski M, Barnas J (2000) Coherent tunneling in ferromagnetic planar junctions: role of thin layers at the barriers. J Appl Phys 88:5230
123. Majumdar K, Hershield S (1998) Magnetoresistance of the double-tunnel-junction Coulomb blockade with magnetic metals. Phys Rev B 57:11521
124. Bartass YV, Nazarov JI, Bauer GEW (1999) Spin accumulation in small ferromagnetic double-barrier junctions. Phys Rev B 59:93
125. Imamura H, Takahasi S, Maekawa S (1999) Spin-dependent Coulomb blockade in ferromagnet/normal-metal/ferromagnet double tunnel junctions. Phys Rev B 59:6017
126. Zeng ZM, Feng JF, Wang Y, Zhang XG, Han XF, Zhan WS, Zhang Z (2006) Probing spin-flip scattering in ballistic nanosystems. Phys Rev Lett 97:106605
127. MacLaren JM, Zhang X-G, Butler WH (1997) Validity of the Julliere model of spin-dependent tunneling. Phys Rev B 56:11827
128. Jedema J, Filip AT, van Wees BJ (2001) Electrical spin injection and accumulation at room temperature in an all-metal mesoscopic spin valve. Nature 410:345
129. Barnas J, Weymann I (2008) Spin effects in single-electron tunneling. J Phys Condens Matter 20:423202
130. Fettar F, Lee S-F, Petroff F, Vaures A, Holody P, Schelp LF, Fert A (2002) Temperature and voltage dependence of the resistance and magnetoresistance in discontinuous double tunnel junctions. Phys Rev B 65:174415
131. Yakushiji K, Ernult F, Imamura H, Yamane K, Mitani S, Takanashi K, Takahashi S, Maekawa S, Fujimori H (2005) Enhanced spin accumulation and novel magnetotransport in nanoparticles. Nat Mater 4:57
132. Feng JF, Kim T-H, Han XF, Zhang X-G, Wang Y, Zou J, Yu DB, Yan H, Li AP (2008) Space-charge trap mediated conductance blockade in tunnel junctions with half-metallic electrodes. Appl Phys Lett 93:192057
133. Liu YW, Zhang ZZ, Freitas PP, Martins JL (2003) Current-induced magnetization switching in magnetic tunnel junctions. Appl Phys Lett 82:2871

134. Wen ZC, Wei HX, Han XF (2007) Patterned nanoring magnetic tunnel junctions. Appl Phys Lett 91:122511
135. Wei HX, He J, Wen ZC, Han XF, Zhan W, Zhang S (2008) Effects of current on nanoscale ring-shaped magnetic tunnel junctions. Phys Rev B 77:134432
136. Miltat J, Albuquerque G, Thiaville A, Vouille C (2001) Spin transfer into an inhomogeneous magnetization distribution. J Appl Phys 89:6982
137. Wei HX, Zhu FQ, Han XF, Wen ZC, Chien CL (2008) Current-induced multiple spin structures in 100-nm nanoring magnetic tunnel junctions. Phys Rev B 77:224432
138. Freitas PP, Cardoso S, Sousa R, Ku W, Ricardo F, Virginia C, Conde JP (2000) Spin dependent tunnel junctions for memory and read-head applications. IEEE Trans Magn 36:2796
139. Song D, Nowak J, Larson R, Kolbo P, Chellew R (2000) Demonstrating a tunneling magneto-resistive read head. IEEE Trans Magn 36:2545
140. Kobayashi K, Akimoto H (2006) TMR film and head technologies. FUJITSU Sci Tech J 42:139
141. Mao SN et al (2006) Commercial TMR heads for hard disk drives: characterization and extendibility at 300 Gbit/in^2. IEEE Trans Magn 42:97
142. Tondra M, Daughton JM, Wang D, Beech RS, Fink A, Taylor JA (1998) Picotesla field sensor design using spin-dependent tunneling devices. J Appl Phys 83:6688
143. Pannetier M, Fermon C, Le Goff G, Simola J, Kerr E (2004) Femtotesla magnetic field measurement with magnetoresistive sensors. Science 304:1648
144. Shen W-F, Liu X-Y, Mazumdar D, Xiao G (2005) In situ detection of single micron-sized magnetic beads using magnetic tunnel junction sensors. Appl Phys Lett 86:253901
145. Piedade M, Sousa LA, de Almeida TM, Germano J, da Costa BD, Lemos JM, Freitas PP, Ferreira HA, Cardoso FA (2006) A new hand-held microsystem architecture for biological analysis. IEEE Trans Circuit Syst I Regul Pap 53:2384
146. Shen W, Schrag BD, Carter MJ, Xiao G (2008) Quantitative detection of DNA labeled with magnetic nanoparticles using arrays of MgO- based magnetic tunnel junction sensors. Appl Phys Lett 93:033903
147. van Dijken S, Jiang X, Parkin SSP (2002) Room temperature operation of a high output current magnetic tunnel transistor. Appl Phys Lett 80:3364
148. van Dijken S, Jiang X, Parkin SSP (2003) Comparison of magnetocurrent and transfer ratio in magnetic tunnel transistors with spin-valve bases containing Cu and Au spacer layers. Appl Phys Lett 82:775
149. Parkin SSP, Jiang X, Kaiser C, Panchula A, Roche K, Samant M (2003) Magnetically engineered spintronic sensors and memory. Proc IEEE 91:661
150. Black WC Jr, Das B (2000) Programmable logic using giant-magnetoresistance and spin-dependent tunneling devices (invited). J Appl Phys 87:6674
151. Ney A, Pampuch C, Koch R, Ploog KH (2003) Programmable computing with a single magnetoresistive element. Nature 425:485
152. Han XF, Wen ZC, Wang Y, Wang L, Wei HX (2008) Nano-scale patterned magnetic tunnel junction and its device applications. AAPPS Bull 18:24
153. Chua LO (1971) The missing circuit element. IEEE Trans Circuit Theory 18:507
154. Strukov DB (2008) The missing memristor found. Nature 453:80
155. Krzysteczko P (2009) Memristive switching of MgO based magnetic tunnel junctions. Appl Phys Lett 95:112508
156. Butler WH, Zhang X-G, Schulthess TC, MacLaren JM (2001) Spin-dependent tunneling conductance of Fe|MgO|Fe sandwiches. Phys Rev B 63:054416
157. Parkin SSP, Kaiser C, Panchula A, Rice PM, Hughes B, Samant M, See-Hun Yang (2004) Giant tunnelling magnetoresistance at room temperature with MgO (100) tunnel barriers. Nat Mater 3:862
158. Yuasa S, Nagahama T, Fukushima A, Suzuki Y, Ando K (2004) Giant room-temperature magnetoresistance in single-crystal Fe/MgO/Fe magnetic tunnel junctions. Nat Mater 3:868

159. Ikeda S, Hayakawa J, Ashizawa Y, Lee YM, Miura K, Hasegawa H, Tsunoda M, Matsukura F, Ohno H (2008) Tunnel magnetoresistance of 604 % at 300 K by suppression of Ta diffusion in CoFeB/MgO/CoFeB pseudo-spin-valves annealed at high temperature. Appl Phys Lett 93:082508
160. Wei S-H, Zhang SB (2001) First-principles study of cation distribution in eighteen closed-shell $A^{II}B2^{III}O4$ and $A^{IV}B2^{II}O4$ spinel oxides. Phys Rev B 63:045112
161. Sukegawa H et al (2010) Tunnel magnetoresistance with improved bias voltage dependence in lattice-matched Fe/spinel MgAl2O4/Fe(001) junctions. Appl Phys Lett 96:212505
162. Zhang J, Han XF, Zhang XG Spinel as spin-filter barrier for magnetic tunnel junctions (Unpublished)
163. Ikeda S, Miura K, Yamamoto H, Mizunuma K, Gan HD, Endo M, Kanai S, Hayakawa J, Matsukura F, Ohno H (2010) A perpendicular-anisotropy CoFeB–MgO magnetic tunnel junction. Nat Mater 9:721
164. Mizukami S, Wu F, Sakuma A, Walowski J, Watanabe D, Kubota T, Zhang X, Naganuma H, Oogane M, Ando Y, Miyazaki T (2011) Long-lived ultrafast spin precession in manganese alloys films with a large perpendicular magnetic anisotropy. Phys Rev Lett 106:117201